University of Alberta

Addition Reactions of Olefins to Asphaltene Model
Compounds

by

Samuel David Cardozo D'Armas

A thesis submitted to the Faculty of Graduate Studies and Research
in partial fulfillment of the requirements for the degree of

Master of Science

in

Chemical Engineering

Department of Chemical and Materials Engineering

ABSTRACT

Two alkyl-bridged aromatic compounds, with molecular weights of 899.70 g/mol and 1127.99 g/mol, were thermally cracked with 1-hexadecene, 1-octadecene, or *trans*-stilbene, in a batch microreactor at 375–430 °C for 15 to 45 min. The objective of the study was to investigate the kinetics of the addition reactions between the olefins and asphaltene model compounds. Reaction products were analyzed by gas chromatography, high-performance liquid chromatography, matrix-assisted laser desorption/ionization mass spectrometry (MALDI-MS), and proton nuclear magnetic resonance (^{1}H NMR) spectroscopy. Kinetic data indicate a first-order reaction in model compound concentration, with energetics consistent with a free-radical chain mechanism. Tandem MS/MS and ^{1}H NMR spectra of the products are consistent with olefin addition through the alkyl bridge of the bridged aromatics. The results imply that the addition products are able to abstract hydrogen to give detectable products faster than they decompose, and that they can react even more readily than the parent compounds.

ACKNOWLEDGEMENTS

TABLE OF CONTENTS

LIST OF TABLES

LIST OF FIGURES

NOMENCLATURE

A	Arrhenius pre-exponential factor
$[C]$	Addition product mass concentration
δ	NMR chemical shift, measured in ppm
E_a	Apparent Arrhenius activation energy
f_i	Fugacity of component i
f_i^0	Fugacity of component i at a standard reference state
f_o	Olefin fugacity
k	First-order rate constant
k_1	Rate constant for the parent radical-olefin addition step
k_2	Rate constant for consumption of the addition product
k_{abs}	Rate constant for hydrogen abstraction
k_{add}	Rate constant for radical addition
P	Pressure
P_c	Critical pressure
P_{sat}	Saturation pressure
P^0	Pressure at a standard reference state
$[\dot{P}]$	Parent radical concentration
$[P]$	Parent compound concentration
$[P]_o$	Parent compound concentration at t = 0
R	Universal gas constant
t	Time
T	Temperature
T_c	Critical temperature
T_r	Reduced temperature
μ_i	Chemical potential of component i
μ_i^L	Chemical potential of component i in the liquid phase
μ_i^V	Chemical potential of component i in the vapor phase
μ_i^0	Chemical potential of component i at a standard reference state
ν	Volume
ω	Acentric factor
X	Conversion

CHAPTER 1:

Introduction and Background

1.1   Introduction

Over the past decades, much attention has shifted towards oil sands bitumen and heavy oils due to the increasing global demand for energy that cannot be satisfied with conventional petroleum resources.[1] Bitumen is a naturally occurring viscous and chemically complex mixture of hydrocarbons mainly obtained from surface mining and in situ production of oil sands.[2] Raw bitumen extracted from the oil sands is a less desirable petroleum resource due to its low API gravity, high viscosity, and high content of unwanted material, which includes high levels of sulfur and nitrogen compounds, heavy metals, solids, and over 50% of vacuum residue.[3] Here is where bitumen upgrading comes into action, with the goal of enhancing its marketability by producing a higher quality synthetic crude oil of increased value.

During the upgrading process, the focus is on the thermal conversion of the vacuum residue to lighter molecules in order to maximize distillates. The vacuum residue is a complex mixture of large and heavy chemical species. The asphaltenes fraction within the residue receives most of the attention, probably due to its chemical complexity, reactivity during processing, and tendency to aggregate. Thermal cracking of the vacuum residue is controlled by a free-radical chain mechanism, which produces olefins in the β-scission steps.[4] These unsaturated compounds can then participate in radical addition reactions in the liquid phase and generate intermediate radicals that can further react or stabilize via hydrogen abstraction, ultimately leading to the formation of higher molecular weight material and coke.

With the continuing growth in the production of synthetic crude oils, further understanding of the chemistry of cracking and coking of heavy residues is needed. The development of new technologies, and improvement of existing ones, relies on the knowledge of the transformations that occur under upgrading conditions. Over the past years, effort has been aimed towards synthesizing[5-9] and studying asphaltene model compounds for bitumen to gain insights into the main reaction pathways for thermal cracking, including the addition reactions that lead to coke formation,[10-13] and the association behavior of asphaltenes in solution.[5,14-18] Though research on the main pathways for addition is better documented, work probing their kinetics at temperatures relevant to bitumen upgrading is scarce. Consequently, in this study we investigate the kinetics of the addition reactions of olefins to model compounds for asphaltenes.

1.2   Objectives

- Define kinetics of the addition reactions, estimate reaction rate constants, and assess consistency with experimental observations

- Establish which step is rate-limiting in the formation of the asphaltene-olefin addition product (olefin addition reaction vs. subsequent hydrogen abstraction)

1.3   Background

The properties, chemistry, and thermal behavior of the heavier, non-distillable fraction of bitumen must be studied if there is to be any hope of overcoming some of the current challenges and shortcomings facing the Canadian oil sands industry. The asphaltenes, by definition, are a solubility class that comprise a significant portion of the vacuum residue and pose many difficulties in extraction, transportation, and downstream upgrading processes. In this section, some of the relevant features and properties of asphaltenes are summarized (such as molecular weight distribution, molecular architecture, and heavy metal composition), followed by an overview of thermal cracking reactions and processes. Emphasis is made on radical addition reactions due their relevance to the present project.

2

1.3.1 Asphaltenes: An overview

Asphaltenes, the heaviest fraction of bitumen and heavy oils, are an extremely complex mixture of polycyclic aromatic hydrocarbons (PAHs), sulfur, nitrogen, and organometallic compounds, defined as the oil fraction soluble in toluene but insoluble in paraffinic solvents, such as n-pentane or n-heptane.[3] The solubility definition of asphaltenes generates a broad distribution of molecular structures, rich in heteroatoms (such as oxygen, nitrogen and sulfur), polar groups, and heavy metals (such as vanadium and nickel), with a high degree of heterogeneity and complexity,[19] and despite substantial research, no general consensus exists on a representative chemical structure for asphaltenes. Nevertheless, an overall agreement on the approximate range of molecular weights of the asphaltenes does appear to exist, and the molar mass of individual components in any asphaltene would typically be in the range of 500–2000 Da, extending up to approximately 3000 Da.[20]

Two structural models for asphaltenes have been proposed and are still under much debate: the archipelago model[21-23] versus the island model[24,25] (also known as continental or pericondensed model). A representative molecular structure of an asphaltene following the archipelago motif is shown in Figure 1-1, composed of polycyclic aromatic cores and cycloalkyl groups linked mainly via alkyl bridges, which tend to be complex iso-paraffins and sulfur containing compounds. The alternative island model is based on a highly alkylated condensed polycyclic aromatic core, usually containing 5 or more fused aromatic rings, such as those shown in Figure 1-2.

The most recent studies[19,26-28] provide a strong support for significant concentrations of a multicore archipelago structure; for example, a study by Rueda et al.[19] shows that cracking of a wide range of asphaltenes from different geological basins gave high yield of 1−3 ring aromatic molecules, suggesting an important presence of small bridged fragments. Similarly, Karimi et al.[27] also obtained quantitative evidence of bridged structures in the asphaltenes by thin film pyrolysis. Analysis of the liquid products showed the existence of a wide range of chemical structures including paraffins, olefins, naphthenes, aromatics, thiophenes, sulfides, and nitrogen-containing compounds, and that the majority of these products consisted of structures containing 1−4 saturated and/or aromatic rings. The evidence suggests that archipelago structures are significant

in many crude oils; therefore, the focus should be on how such architectures are created or destroyed during processing, in parallel to the behavior of smaller alkyl-aromatic compounds.
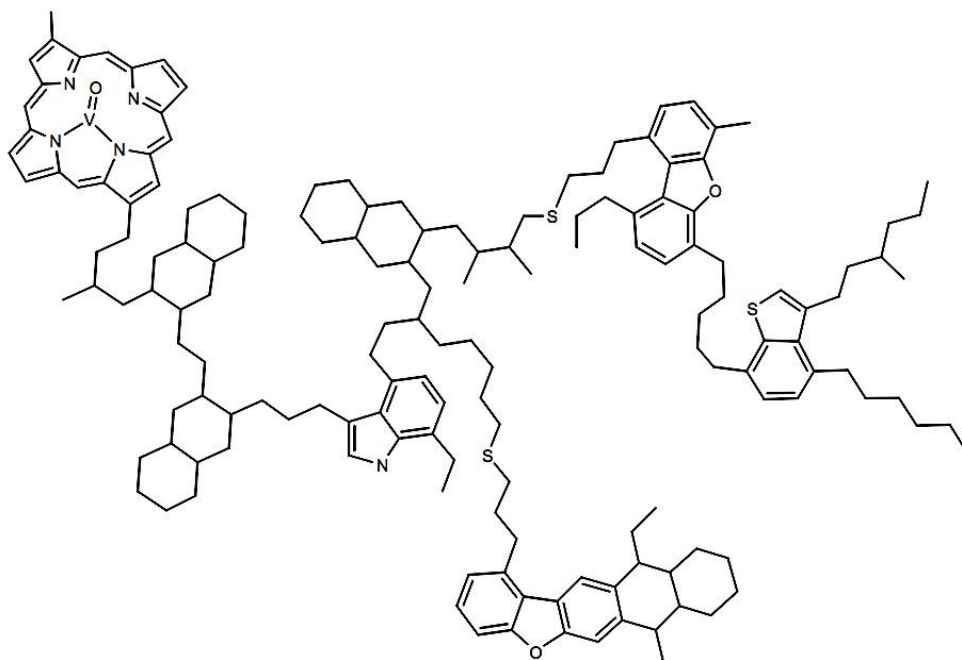
Figure 1-1. Representative molecular structure of an Athabasca asphaltene,[22] reduced molecular weight MW = 2380 g/mol

Asphaltenes are problematic because they have a high tendency of forming coke during upgrading,[29] they precipitate out in pipelines, plug lines, deposit in heat exchangers and on reactor surfaces, and foul catalysts during crude oil processing.[30-32] Furthermore, the heavy metals in the asphaltenes--the most metal-rich fraction of bitumen--are quite difficult to remove and tend to cause severe problems during processing and utilization, such as catalyst poisoning in catalytic cracking and hydrotreating.[21,33] These metals, mainly Ni and V, are present in crude oil or bitumen at concentrations up to 1320 ppm, depending upon the source,[34,35] and occur predominantly as substituted porphyrins or tetrapyrrole-like structures in the asphaltenes,[36-40] some more structurally elaborated than others. Even small amounts of metals in the feed for catalytic cracking can affect the catalyst activity and result in increased coke and gas formation and reduced product yields.

4
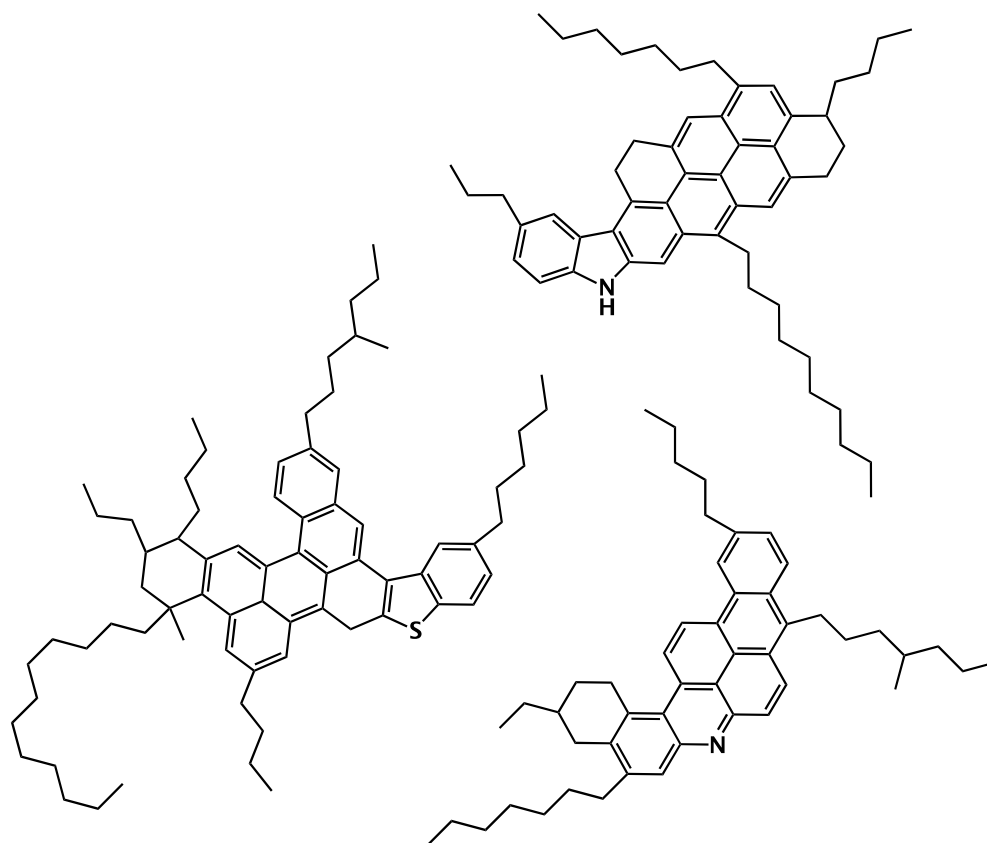
Figure 1-2. Representative structures of proposed continental asphaltene molecules[24]

The porphine macrocycle, produced by the condensation of four pyrrole rings through four methine groups, is shown in Figure 1-3, and it is in the central 4-N cavity where the structure coordinates to the metal ions. The presence of these compounds in crude oil, heavy oil, and bitumen is linked to the biological origin of fossil fuels,[41-46] and their unique physicochemical properties depend upon the nature, distribution, and extent of substitution of functional groups on the porphyrin backbone,[38,47] which are expected to impact the thermal stability and reaction pathways during thermal cracking.[48] Considering that the vacuum residue and asphaltenes, and petroleum in general, are comprised of hundreds of thousands of components,[49] probing the thermal cracking behavior of representative compounds for these fractions, such as metalloporphyrins, is essential for our ever-growing understanding of these materials.
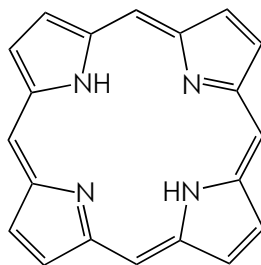
Figure 1-3. Molecular structure of porphine macrocycle

1.3.2   Addition reactions during thermal cracking

The core step in any commercial upgrading process for residues is cracking the large molecules into smaller, more volatile fragments. Petroleum fractions undergo significant cracking at temperatures above ca. 400 °C.[20] Industrial processes upgrade the heavy fractions at variable severities, ranging from mild conditions to reduce the viscosity of the feedstock in visbreaking operations,[50] to severe conditions in ultrapyrolysis processes to obtain high yields of olefins and light gases,[51] but regardless of the process, the underlying chemistry is the same; thermal cracking of heavy oils and vacuum residues is controlled by a free-radical chain mechanism, illustrated in Figure 1-4, showcasing the diversity of the radical reactions that determine the kinetics, thermodynamics, and outcome of these upgrading processes.

The initiation step consists of the homolytic cleavage of the chemical bonds of the molecules to produce radical species that can propagate through many scission and hydrogen abstraction steps before terminating. The minimum energy required to break these covalent bonds in the initiation step is termed bond dissociation energy (BDE) and depends on the nature of the bond, as illustrated in Table 1-1. At the typical temperatures for heavy oil/bitumen upgrading of ca. 400–540 °C,[52] aromatic C–C bonds are not expected to crack due to the high resonance stabilization energy of the π–electrons, but aliphatic C–C bonds do spontaneously cleave at these elevated temperatures without the use of a catalyst. This first initiation step is the most energy intensive, but the high energy requirement is compensated by the low activation energies of the subsequent steps and make the overall reaction energetically feasible;[4] hence, the activation energies for cracking are considerably lower. For example, Olmstead and Freund[53] determined an activation energy for the thermal

cracking of Arab Heavy and Cold Lake vacuum residues of 213–217 kJ/mol, which is much lower than any BDE in Table 1-1, thus supporting a free-radical chain mechanism.

Initiation $\qquad$ R–R' $\xrightarrow{k_{in}}$ R$^{\bullet}$ + R'$^{\bullet}$

Propagation:

Hydrogen abstraction $\quad$ β$_j^{\bullet}$ + R$_j$H $\xrightarrow{k_{ij}}$ β$_j$H + R$_j^{\bullet}$

β-scission $\qquad$ R–C$^{\bullet}$–C–β$_j$ $\xrightarrow{k_i}$ R–C=C + β$_j^{\bullet}$

Radical addition $\qquad$ R$_i^{\bullet}$ + C=C–R$_k$ $\xrightarrow{k_a}$ R$_i$–C–C$^{\bullet}$–R$_k$

Radical rearrangement $\;$ R–C$^{\bullet}$–C–β$_j$ $\xrightarrow{k_r}$ R$_i^{\bullet}$

Termination:

Radical recombination $\;$ R$_i^{\bullet}$ + R$_j^{\bullet}$ $\xrightarrow{k_c}$ R$_i$–R$_j$

Disproportionation $\qquad$ R$_i^{\bullet}$–R$_j$ + R$_k^{\bullet}$ $\xrightarrow{k_d}$ R$_i$=R$_j$ + R$_k$H

Olefin removal

Donor solvent $\qquad$ R–C=C + R'H$_2$ $\xrightarrow{k_s}$ R–C–C + R'

Catalytic $\qquad$ R–C=C + H$_2$ $\xrightarrow{k_h}$ R–C–C

Aromatic hydrogenation $\quad$ R' + H$_2$ $\xrightarrow{k_a}$ R'H$_2$
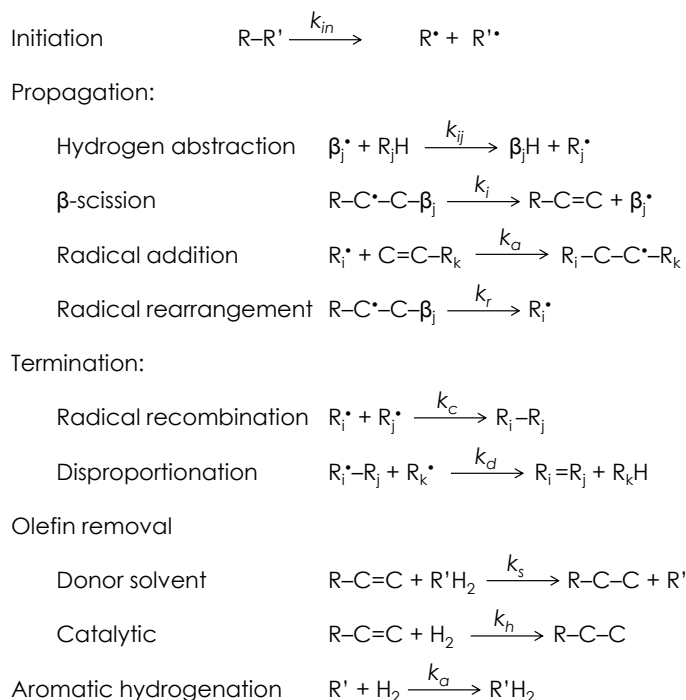
Figure 1-4. Chain reaction mechanism for liquid-phase cracking (adapted from Gray and McCaffrey[4]). Hydrogen atoms are omitted for clarity.

Table 1-1. Bond disassociation energies (BDE) from McMillen and Golden[54]

Chemical bond	Representative bond	BDE at 298 K, kJ/mol
	nC$_3$H$_7$–C$_2$H$_5$	336 ± 8
C–C	CH$_3$–CH$_2$C$_6$H$_5$	317 ± 4
	CH$_3$–C$_6$H$_5$	426 ± 8
	H–C$_2$H$_5$	411 ± 4
C–H	H–C$_6$H$_5$	464 ± 8
	H–CH$_2$C$_6$H$_5$	368 ± 4
C–S	CH$_3$S–C$_2$H$_5$	307 ± 8
C–N	C$_2$H$_5$–NH$_2$	342 ± 8
C–O	C$_2$H$_5$O–C$_2$H$_5$	344 ± 4

Both β-scission and hydrogen abstraction are fundamental steps for the propagation of free radicals. One problem is that the cracking of radicals via β-scission leads to the formation of an olefin product. These unsaturated compounds can then participate in radical addition reactions, and further polymerization could lead to phase separation and coke formation.[4] The best known use of free radical addition to olefins is probably polymerization, but such reactions are carried out at relatively low temperatures, and even those commercial processes that operate at higher temperatures (>180 °C and often >250 °C),[55] are still nowhere close enough to the range of temperatures relevant to conversion of heavy oils and bitumen. However, even under commercial residue processing conditions, radical addition remains thermodynamically feasible, and of course, kinetically accessible.[4,56] Thus olefins undergo addition reactions to cracked fragments and to parent radicals, and to some extent polymerize to higher molecular weight species. At high conversions, this disproportionation leads to the formation of high yields of light gases and insoluble carbon-rich coke material.

Studies by Khorasheh and Gray[57-59] showed that α-olefins formed from cracking of n-hexadecane (n-C$_{16}$) undergo addition reactions in the liquid phase, leading to the formation of larger structures. Likewise, Wu et al.[60] also observed the formation of branched alkanes with higher carbon atoms than the starting material during pyrolysis of n-hexadecane, but only at the high molecular density of liquid-phase cracking. At the dilute conditions of gas phase reactions, where the density of the reacting species is low, unimolecular β-scission is dominant, in contrast to reactions in condensed conditions, such as liquid phase or high-pressure gas phase, where bimolecular reactions are favored, e.g., hydrogen abstraction and radical addition. Since the asphaltenes transition to a liquid melt prior to reaching reaction temperatures,[61] thermal cracking of this fraction occurs predominantly in the liquid-phase. Herein lies the importance of studying the liquid-phase thermal cracking of petroleum components, since at these conditions asphaltenes are expected to undergo addition reactions to build heavier products, and eventually, coke.[62]

One method to investigate the addition reactions in these highly complex asphaltene systems is by probing the behavior of defined synthetic compounds that incorporate substructures and functional groups that are known to be

present in the asphaltenes, within the established range of molecular weights, and with sufficiently high boiling points to ensure liquid-phase cracking. The most recent studies of this nature were carried out by Alshareef et al.[10,11] using a variety of asphaltene model compounds with molecular weights that range from 459 to 763 g/mol, most of which had a molecular architecture as depicted in Figure 1-5 (three-island archipelago consisting of two pyrenyl groups joined to a central aromatic or heteroaromatic group by ethano bridges). The central aromatic group included structures such as benzene, biphenyl, pyridine, thiophene, and dibenzofuran. Cracking of these model compounds at 350–420 °C showed the formation of addition products with molecular weights higher than that of the starting compounds, fully consistent with a free-radical mechanism involving radical addition to cracked products containing unsaturated bonds. Also, their data suggest that alkyl-alkyl and alkyl-aryl additions were dominant in building the larger product molecules, and that coke yield is controlled by the rate of addition reactions and the stability of the addition products.
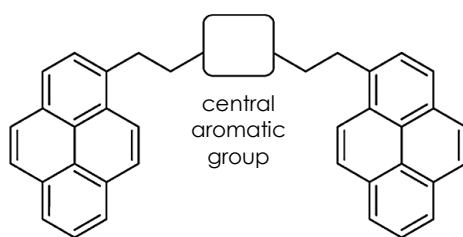
Figure 1-5. General structure of the pyrene-based model compounds studied by Alshareef et al.[11]
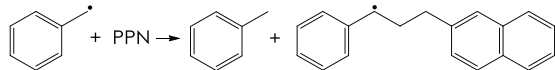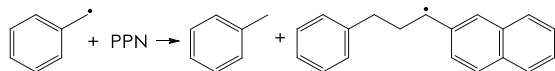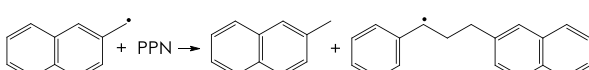
Clearly, kinetic data and rate estimates for the addition reactions would improve our overall understanding of the underlying chemistry of coking processes. The formation of addition products during cracking would depend on the rate of radical addition to unsaturated molecules and of the subsequent hydrogen abstraction, which would dictate how quickly the formed radical addition product could stabilize. Assessing the relative importance of these competitive processes requires some prior knowledge of their Arrhenius parameters, of the concentrations involved, and of the factors controlling them. Although no significant amount of kinetic work has been done with compounds

relevant to the asphaltene fraction, Table 1-2 and Table 1-3 summarize some of the Arrhenius rate parameters that have been previously reported for radical addition reactions and hydrogen abstraction, respectively.

Table 1-2. Rate parameters for free-radical addition reactions

Source	Reaction		E_a, kJ/mol	log(A, L mol^{-1} s^{-1})
Thermal cracking of n-C$_{16}$[57]	n-alkyl radical + α-olefin → higher alkyl radical		29.3	7.2–10
Thermal cracking of n-C$_{16}$ in toluene[58]	Ph$^\bullet$CH$_2$ + α-olefin → n-alkylbenzene radical Ph is phenyl		29.3	6.3
n-C$_{16}$ decomposition (liquid phase)[63]	$^\bullet$R + 1-alkene → $^\bullet$R'		20.9	
Pyrolysis of hexane[64]	e.g. C$_6$H$_{13}$ + C$_3$H$_6$ → C$_9$H$_{19}$ (simplified mechanism)		29.3	8.8
Pyrolysis of hexane[65]	Gas phase (~36 addition reactions)		28.0–40.6	10.0–12.95
Pyrolysis of butylbenzene[66]	Ph$^\bullet$CH$_2$ + CH$_2$=CHCH$_3$ → PhCH$_2$CH$_2$$^\bullet$CHCH$_3$		31.8	7.78
	$^\bullet$CH$_3$ + CH$_2$=CH$_2$ → CH$_3$CH$_2$$^\bullet$CH$_2$		32.2	8.52
Reactions of free radicals relevant to pyrolysis (review)[56]	$^\bullet$CH$_2$(CH$_2$)$_4$CH$_3$ + R-CH=CH$_2$ → CH$_3$(CH$_2$)$_6$$^\bullet$CH-R		29.3–33.5	
Alkyl radical addition to the C=C bond of olefins[67]	Primary alkyl radical + terminal olefin		32±2	
	Secondary alkyl radical + terminal olefin		25±2	
	Tertiary alkyl radical + terminal olefin		18±2	
Liquid phase addition of radicals to terminal olefins[68]	Ph$^\bullet$CH$_2$ + CH$_2$=C(X,Y)	(H,Et)	39.6	
		(H,Ph)	30.9	
		(Me,Ph)	31.6	
		(Ph,Ph)	27.7	
Addition of carbon-centered radicals to alkenes in solution[69]	Ph$^\bullet$CH$_2$ + CH$_2$=C(X,Y)	(H,Et)	39.3	7.5±0.5 to 8.5±0.5 for small alkyl radicals
		(H,Ph)	31.0	
		(Me,Ph)	31.4	
		(Ph,Ph)	28.9	
	Ph$^\bullet$CH$_2$ + styrene		31.0	8.5

Table 1-3. Rate parameters for hydrogen abstraction (H-abs) reactions

Source	Reaction	E_a, kJ/mol	log(A, L mol^{-1} s^{-1})
Pyrolysis 2-(3-phenyl propyl) naphthalene (PPN)[70]		59.4	8.0 (for all H-abs rates)
		58.6	
		60.2	
Pyrolysis of 1-methylpyrene and 1-ethylpyrene[71]	$PyCH_2CH_3 + Py^{\bullet}CH_2 \rightarrow Py^{\bullet}CHCH_3 + PyCH_3$ Py is pyrenyl	64.9	8.8
Pyrolysis of 1-dodecylpyrene (1-DDP)[72]	$Py^{\bullet}CH_2 + 1\text{-DDP} \rightarrow PyCH_3 + \gamma\text{-DDP radical}$	63.2	
	n-decyl radical $+ 1\text{-DDP} \rightarrow C_{10}H_{22} + \alpha\text{-DDP radical}$	29.3	8
	n-dodecyl radical $+ 1\text{-DDP} \rightarrow C_{12}H_{26} + \alpha\text{-DDP radical}$	29.3	
n-C$_{16}$ decomposition (liquid phase)[63]	$^{\bullet}R + n\text{-}C_{16}H_{34} \rightarrow R\text{-}H + {^{\bullet}C_{16}H_{33}}$	49.4	
Thermolysis of Py(CH$_2$)$_{20}$Py[73]	$Py^{\bullet}CH(CH_2)_{19}Py + Py(CH_2)_{20}Py \rightarrow Py(CH_2)_{20}Py + PyCH_2CH_2{^{\bullet}}CH(CH_2)_{17}Py$	31.8	9.4
Thermal cracking n-C$_{16}$ in toluene[58]	(i,j) refers to radical type, i, and hydrogen type, j: $\quad k_{(abs)(s,Bz)}$	50.4	7.5
	$k_{(abs)(p,Bz)}$	42.0	8.6
	$k_{(abs)(Bz,p)}$	58.6	6.6
	p, primary $\quad k_{(abs)(Bz,s)}$ s, secondary	49.0	6.6
	Bz, benzyl, benzylic H $\quad k_{(abs)(Bz,Bz)}$	70.7	6.5

A general observation is that radical addition reactions have quite low activation energies (8–34 kJ/mol),[57] and that rate constants for these bimolecular reactions tend to vary with radical and olefin substitution, decreasing with increasing radical size due to steric effects.[69,74] In the case of radical addition in the gas phase, rate constants appear to be smaller, suggesting that gas-phase activation energies seem to be higher by several kJ/mol.[69]

1.3.3 Operating conditions of industrial upgrading processes

Commercial upgrading processes target the vacuum residue and asphaltene fractions of heavy oils and bitumen, and are capable of dealing with the high heteroatom content and the high coke-forming tendency of these materials. Two of the main processes used in upgrading heavy bitumen fractions are coking, which includes both delayed and fluid coking technologies, and hydroconversion. Although hydroconversion processes give high volumetric yield of liquid products with little to no coke formation, they are expensive to operate due to the high cost of hydrogen and catalyst. In contrast, coking processes have significantly lower operating costs but yield lower amounts of liquid products due to the high levels of coke formation.[75] Regardless of the commercial upgrading processes selected, however, conversion of the feed to liquid fuels relies on heat, whether hydrogen and a catalyst are used or not.

In delayed coking operations (semi-batch process), the feed is heated to ca. 500 °C and accumulated in a coke drum, where thermal cracking in the liquid phase over long reaction times converts the feed into light ends (gases), liquid distillates, and solid coke. Similarly, fluid coking processes operate at high temperatures, in the range of 510–550 °C, but with much shorter residence times. In this continuous process, however, the feed is sprayed onto a fluid bed of heated coke particles which provide the heat for cracking of the feed. In terms of product distributions, delayed and fluid coking processes give similar liquid yields, but fluid coking has a lower net coke production. Table 1-4 gives the operating conditions for a variety of other industrial processes associated with heavy oil/bitumen upgrading. Thermal cracking reactions during these industrial processes will drive addition reactions in the liquid phase, as previously discussed, leading to the formation of higher molecular weight material at the expense of lighter distillable components.

Table 1-4. Operating conditions of industrial heavy oil and bitumen upgrading processes (from Cartlidge et al.[52])

Process	Temperature, °C	Pressure, MPa	Reactor type
Processing with coke rejection			
Solvent de-asphalting	150–180	4	Solvent extractor
ROSE	197	3.5	Solvent extractor
Delayed coking	487–510	0.2–0.4	Coking drums
Eureka	420–430	0.1	Coking drums
Flexicoking	510–537	0.1	Fluidized bed
ART	500–540	0.1	Fluidized bed with riser
KK	700–800	0.1	Fluidized bed with steam stripping
Dynacracking	500–540	2.7–4.1	Fluidized bed with 3 zones
RCC	537–622	0.07–0.25	Vented riser
HOC	524–529	0.1	Fluidized catalytic cracker
Processing with coke minimization			
Visbreaking	477–500/427–443	5.17	Coil cracker/Soaker drum
Hydrovisbreaking	377–427	8–9	Soaker drums
HDDC	447–467	2.6–3.1	
HDDV	442–457	2.4–2.8	
DRB	410–460	3.5–5.5	Donor solvent
CANMET Hydrocracking	435–455	13.6	Upflow reactor
VCC	455–464	15–26	Vertical slurry
HDH	451	13–14	Vertical slurry
LC-fining	432	15.5	Ebullated bed
H-oil	454	15.5	Ebullated bed
Tervahlc	410	15	Slurry reactor
Unibon-RCD-BOC	380–420	18	Fixed bed
ABC	410	13.8	Fixed bed

1.3.4 Vapor-liquid equilibrium (VLE)

Process design for upgrading of heavy oils and bitumen requires calculations based on VLE to quantitatively describe the distribution at equilibrium of every component among all the phases present, for example, in separation processes such as distillation. These computations are typically carried out using a process simulator software, which use a set of material-balance, thermodynamic methods, and equations of state to calculate phase behavior. An equation of state (EOS) is a mathematical expression relating pressure, volume, and temperature, and is used to describe the volumetric behavior, the VLE, and the thermal properties of pure substances and mixtures.[76] Due to the complexity of crude oils and bitumen, however, each component cannot be uniquely identified; therefore, oils are characterized by pseudo-components, grouping together components that exhibit similar behavior. This grouping is done by boiling point, so that an oil is characterized as a series of boiling cuts obtained by, for example, simulated distillation or true boiling point distillation. Grouping the oil into pseudo-components is particularly important for EOS-based simulations, and so pseudo-component selection will influence the quality of the fluid characterization.

Equations of state can be divided into two main groups: cubic and non-cubic. Although non-cubic EOS can better describe the volumetric behavior of pure substances, they may not be suitable for complex hydrocarbon mixtures.[77] Therefore, proper selection of thermodynamic models is absolutely necessary for accurate and reliable process simulation. Currently, a number of EOS are commonly used which have shown more reliability in phase equilibrium calculations of heavy oils. One example is the Peng-Robinson[78] equation:

$$P = \frac{RT}{v - b} - \frac{a(T)}{v(v + b) + b(v - b)}$$

(1-1)

where R is the universal gas constant, P is the pressure, T is the temperature, v is the volume, and:

$$a = 0.45724 \, \alpha \, R^2 \, T_c^2 \, P_c^{-1}$$

(1-2)

$$b = 0.07780 \, R \, T_c \, P_c^{-1}$$

(1-3)

$$\alpha^{1/2} = 1 + \kappa(1 - T_r^{1/2})$$

(1-4)

$$\kappa = 0.37464 + 1.54226 \, \omega - 0.26992 \, \omega^2$$

(1-5)

where, T_c is the critical temperature, P_c is the critical pressure, T_r is the reduced temperature, and ω is the acentric factor, defined as follows:

$$\omega = - log_{10}[P_{sat}/P_c]_{Tr=0.7} - 1.0 \qquad (1\text{-}6)$$

where P_{sat} is the saturation pressure at a specified reduced temperature. Consequently, the cubic Peng-Robinson EOS allows for estimation of phase behavior of a component given its critical properties and the acentric factor. Though these equations were generally developed for pure substances, they can be extended to mixtures through the use of mixing rules. In the case of oils, the critical properties and acentric factor must be estimated for the defined pseudo-components. Several correlations are available and are built into the process simulators, and generally require information on the molecular weight, boiling point, and specific gravity of each boiling cut.[75]

Phase equilibria are calculated by equations of state by satisfying the condition of chemical equilibrium. For a two-phase system, the chemical potential of each component in the liquid phase μ_i^L must equal the chemical potential of each component in the vapor phase μ_i^V.[76] However, since chemical potential does not have an immediate equivalent in the physical world, it can be expressed, for example, in terms of fugacity, f_i, which serves as an auxiliary variable linking the more abstract thermodynamic concept of chemical potential with a physical variable, pressure.[79] For an ideal gas, the change in chemical potential $(\mu_i - \mu_i^0)$, in isothermally going from pressure P^0 (at a standard reference state) to pressure P, can be written as:

$$\mu_i - \mu_i^0 = RTln\frac{P}{P^0} \qquad (1\text{-}7)$$

In a general form, for an isothermal change for any component i in any system, solid, liquid, or gas, pure or mixed, ideal or not, Equation (1-7) can be expressed as:

$$\mu_i - \mu_i^0 = RTln\frac{f_i}{f_i^0} \qquad (1\text{-}8)$$

Thus, fugacity can be a considered as a "corrected pressure" that takes into account molecular non-idealities; for a pure, ideal gas, it is equal to the pressure, and for a component in a mixture of ideal gases, it is equal to the partial pressure of that component. Furthermore, the equilibrium condition in terms of

15

chemical potentials can be replaced with an analogous condition in terms of fugacity, so that, for any species i, the fugacities must be the same in all phases at equilibrium. This relation between fugacity and chemical potential provides a more convenient way to apply phase-equilibrium thermodynamics in practical applications.

CHAPTER 2:

Experimental Methods
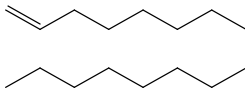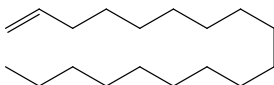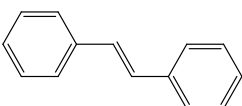
2.1   Chemicals, olefins, and asphaltene model compounds

All the chemicals, olefins, and asphaltene model compounds used in this study are listed in Table 2-1, Table 2-2, and Table 2-3, respectively. Olefins include two alpha-olefins (1-C_{16} and 1-C_{18}), and one aromatic olefin (*trans*-stilbene), and were obtained from commercial suppliers. The asphaltene model compounds consisted of one or two pyrenyl groups linked together by ethano bridges to a central aromatic group – nickel(II) tetraphenylporphyrin (NiTPP). These model compounds follow the archipelago motif, and the abbreviated names used herein are based on the number of 1-ethylpyrene groups in the substrate.

Table 2-1. List of chemicals used in the experiments

Chemical	Manufacturer	Purity and/or grade
Dichloromethane	Sigma-Aldrich Co.	Chromasolv® for HPLC, ≥ 99.9%
Methanol	Sigma-Aldrich Co.	Chromasolv® for HPLC, ≥ 99.9%
Naphthalene	Sigma-Aldrich Co.	≥ 99%
5,10,15,20-tetraphenyl-21H,23H-porphine (TPP)	Sigma-Aldrich Co.	≥ 99%
trans-2-[3-(4-tert-butylphenyl)-2-methyl-2-propenylidene] malononitrile (DCTB)	Santa Cruz Biotechnology, Inc.	≥ 99%
Nitrogen	PRAXAIR Canada Inc.	Ultra High Purity, 5.0
Helium	PRAXAIR Canada Inc.	Ultra High Purity, 5.0

Table 2-2. Olefins used for microreactor experiments
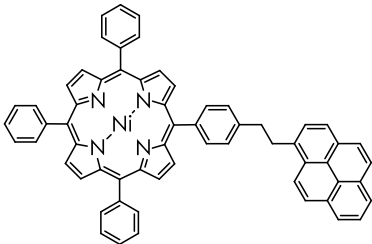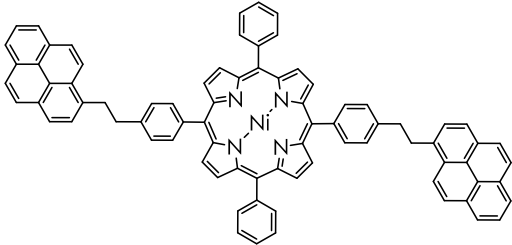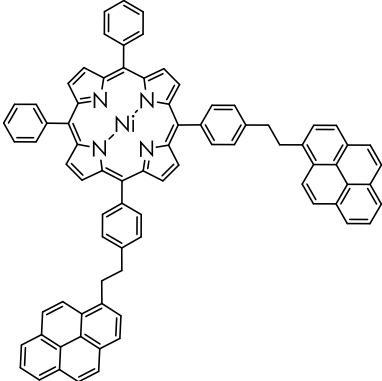
Olefin	Manufacturer	Molecular structure	Molecular weight, g/mol	Purity, %
1-hexadecene 1-C$_{16}$	Sigma-Aldrich Co.		224.43	≥ 99
1-octadecene 1-C$_{18}$	Sigma-Aldrich Co.		252.48	≥ 99.5
trans-stilbene	Acros Organics		180.25	96

Thermal cracking experiments were also performed using a substituted cholestane-naphthoquinoline model compound, shown in Figure 2-1, based on aromatic biomarkers identified in crude oil.[80] However, this model compound proved to be less reactive towards formation of addition products, as observed for other substituted cholestane-benzonquinoline compounds of similar structure,[10,12,81] so kinetic studies for addition were focused using the bridged petroporphyrin model compounds.
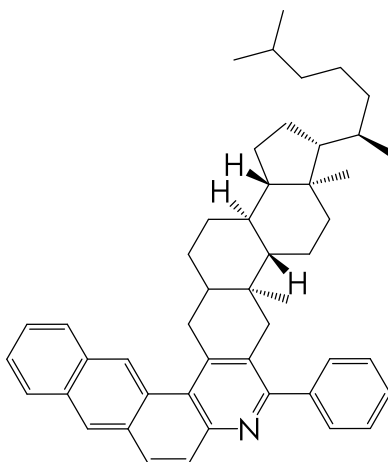
Figure 2-1. Substituted cholestane-naphthoquinoline asphaltene model compound (MW = 647.45 g/mol)

Table 2-3. Asphaltene model compounds investigated

Model compound	Molecular structure	Molecular weight, g/mol	Purity, %
[Et-Py]NiTPP 5,15,20-tris-(phenyl)-10-(4'-(ethylpyrene)-phenyl)-porphyrinato-nickel(II)		899.70	98
2[Et-Py]NiTPP 5,15-bis-(phenyl)-10,20-bis-(4'-(ethylpyrene)-phenyl)-porphyrinato-nickel(II) *trans* isomer	mixture of two isomers: 	1127.99	98
5,20-bis-(phenyl)-10,15-bis-(4'-(ethylpyrene)-phenyl)-porphyrinato-nickel(II) *cis* isomer		1127.99	98

2.2   Thermogravimetric analysis (TGA)

A TA Instruments – Q500 Thermogravimetric analyzer was used to perform TGA of the model compounds in order to estimate and compare their initial cracking kinetics to another series of pyrene-based archipelago model compounds reported elsewhere.[11] For each run, a total of 4–5 mg of the sample was loaded on a platinum pan, heated at 10 °C/min from 25 °C to 500 °C, and then held at 500 °C for 15 min to obtain an approximate value of the microcarbon residue (MCR) content. All experiments were done using nitrogen as purge gas, at a flow rate of 60 mL/min.

2.3   Microreactor experiments

To investigate the kinetics of the addition reactions between the olefins and asphaltene model compounds, thermal cracking experiments were carried out in ¼" stainless-steel batch microreactors under conditions relevant to bitumen upgrading. A schematic of the microreactor, illustrating its components and dimensions, is shown in Figure 2-2.

S.S. Integral Bonnet Needle Valve

S.S. Swagelok Tube Fitting $^1/_{16}$" x $^1/_8$" Reducer

316 S.S. Tubing, $^1/_{16}$" OD 9 cm

S.S. Swagelok Tube Fitting ¼" x $^1/_{16}$" Reducing Union

316 S.S. Tubing, ¼" OD 5 cm

316 S.S. Cap for ¼" OD Tubing
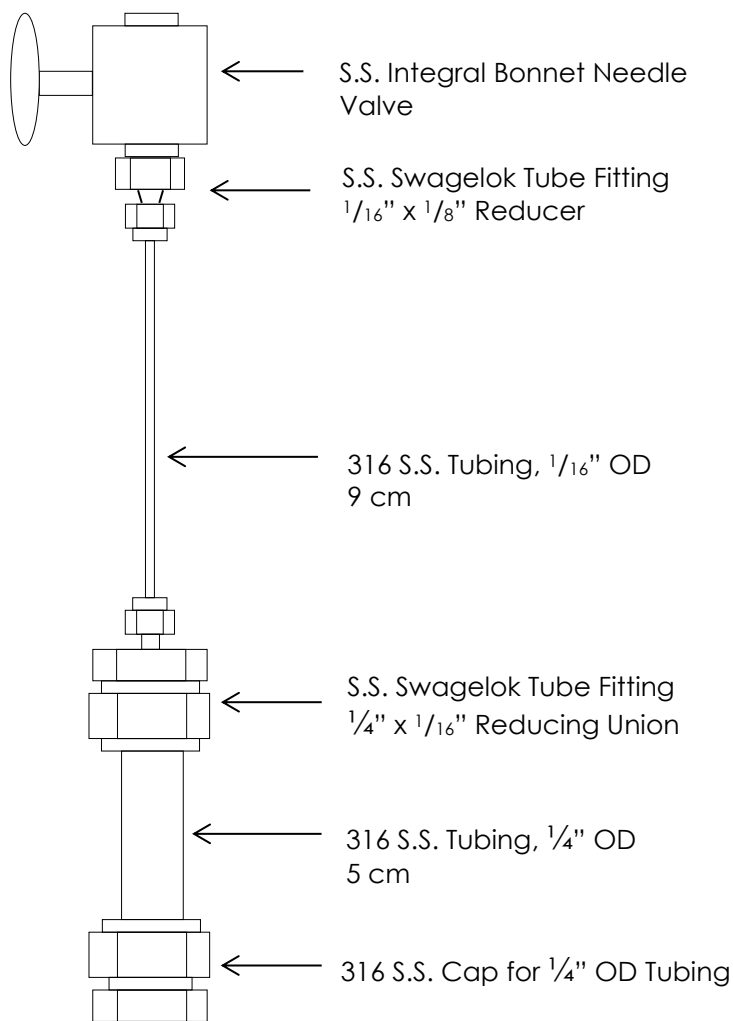
Figure 2-2. Schematic of the ¼" SS batch microreactor (volume < 1 mL)

Typically, a total of 1–2 mg of each model compound was loaded into a 3 x 45 mm one-end-sealed glass liner, which facilitated product recovery and helped avoid any catalytic activity with the reactor walls. The olefin was loaded

into the body of the reactor to prevent carry-over of material when the olefin boils. Figure 2-3 illustrates the distribution of reactants inside the reactor. The amount of olefin loaded, approx. 10–60 mg, was based on calculation of vapor-liquid phase equilibrium to ensure the presence of an olefin liquid phase.
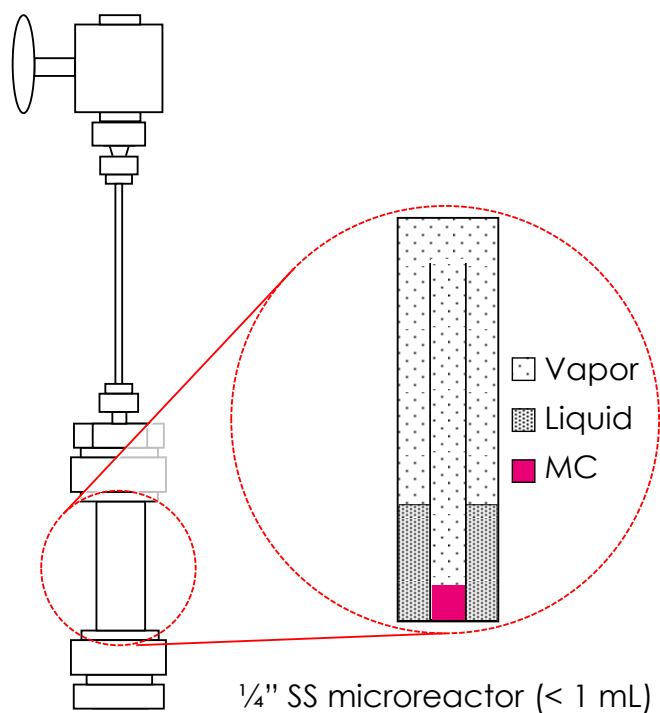
Figure 2-3. Distribution of reactants inside the reactor: model compound (MC) is loaded in a glass liner and the olefin in the body of the reactor. At reaction conditions, the olefin is present in both vapor and liquid phases.

The loaded liner was then placed in the microreactor with the open side up, after which the reactor was sealed, purged with nitrogen at least 5 times, and heated by immersion into a fluidized sand bath (Tecam Fluidized Sand Bath Model No. SBS–4). Fluidization of the sand was achieved through a regulated air flow, which was kept constant at 40% throughout the experiments. Thermal cracking reactions were carried out at 375–430 °C for 15–45 min. At the end of each experiment, the reactor was air-cooled, and the products extracted with dichloromethane and concentrated using a rotary evaporator.

2.4   Sample analysis

Liquid products were analyzed by proton nuclear magnetic resonance spectroscopy, gas chromatography, high-performance liquid chromatography, and/or matrix-assisted laser desorption/ionization mass spectrometry, depending on the purpose of experiment performed.

2.4.1   Proton nuclear magnetic resonance (^{1}H NMR) spectroscopy

^{1}H NMR spectroscopy, along with spectra calculated with MestReNova software,[82] were used in elucidating the location of olefin addition to the model compounds. For spectra collection, approximately 2 mg of sample was dissolved in deuterated dichloromethane (CD_2Cl_2) and transferred into NMR tubes for ^{1}H NMR. The ^{1}H NMR spectrum of samples was then collected on a Varian Inova four-channel 500 MHz Spectrometer at 27 °C.

2.4.2   Gas chromatography (GC)

Analysis by gas chromatography-flame ionization detector (GC-FID) and gas chromatography-mass spectrometry (GC-MS) using a Thermo Scientific Trace GC Ultra gas chromatograph and attached Trace DSQII Mass Spectrometer, allowed identification and quantification of small cracked products (mass-to-charge ratio, $m/z < 300$) in control experiments.

For GC-FID runs, the column was a Thermo TR-5, 7 m x 0.32 mm x 0.25 μm. The GC oven was set at an initial temperature of 30 °C for 1 min, followed by continuous ramping at 10 °C /min to 300 °C, and held at 300 °C until elution was completed. Helium was used as the carrier gas at 2 mL/min in a split mode, with a split flow of 50 mL/min. The FID was operated at 250 °C, with the following gas flows: air at 350 mL/min, hydrogen at 35 mL/min, and make-up gas at 30 mL/min. Injection volume was 1 μL. A small amount of naphthalene (typically 1.0–1.5 mg) that was added to the sample served as internal standard. GC-MS was equipped with a Thermo TR-5MS column, 15 m x 0.25 mm x 0.1 μm, and was run with the same temperature program in a split mode.

2.4.3   High-performance liquid chromatography (HPLC)

Measurement of the model compound concentration after reaction was carried out by an Agilent Technologies 1200 Series High-Performance Liquid Chromatograph. The instrument was equipped with a Zorbax Eclipse PAH column of 4.6 x 150 mm with a C18 phase of 3.5 μm particles. The mobile phase was 65% methanol and 35% dichloromethane (isocratic flow), with a temperature of 23 °C, maximum pressure of 400 bar, and constant flow at 1 mL/min. The UV/Visible detector was set to record at a wavelength of 239 nm and 414 nm.

Injection of samples was automated and set to 0.5 μL injection volumes. TPP was used as an internal standard (circa 0.30–0.40 mg per sample), and calibration curves were made for both porphyrin model compounds. Calibration curves were found to be linear in the signal response (area of peaks) to the concentration of analyte, and can be found in Appendix A.

2.4.4   Matrix-assisted laser desorption/ionization mass spectrometry (MALDI-MS)

An Applied Biosystems SCIEX 4800 *Plus* MALDI TOF/TOF Analyzer was used to carry out MALDI-MS analyses of the reaction mixtures, allowing the detection of cracked products and addition products that are too heavy to elute in a GC (m/z > 300). This instrument also had tandem MS/MS capabilities, which enables further fragmentation of precursor ions of a selected mass-to-charge ratio previously identified in a MALDI-MS spectrum.

Product samples to be analyzed by MALDI-MS and tandem MS/MS analysis were prepared as follows: DCTB matrix solution was made to a concentration of 10 mg/mL in dichloromethane, and vortex-mixed with sub-samples of the reaction solution in a 4:1 (v/v) ratio. To minimize variability due to sub-sampling of the reaction solution, a minimum of 3 sub-samples were prepared this way. Next, 1.0 μL portions of the final mixtures were spotted onto a 384 Opti-TOF 123 x 81 mm stainless steel MALDI plate by Applied Biosystems, minimum of 3 spots per sample, and allowed to dry, leaving an opaque crystal layer. The plate was then magnetically affixed to a stainless steel plate holder and placed into the loading chamber of the instrument. MS data acquisition was carried out in the reflector positive mode, with the laser intensity set between 3050–3300. For tandem MS/MS mode, laser intensity was usually set to 3900.

MALDI-MS and MS/MS spectra shown in this study are representative of the typical spectrum collected for a particular sample. Acquisition and averaging of multiple spectra allowed minimizing shot-to-shot, region-to-region, and sample-to-sample variability due to heterogeneous co-crystallization of the matrix and analyte.[83]

CHAPTER 3:

Results and Discussion

3.1 Thermogravimetric analysis (TGA) of model compounds

In practice, TGA can provide a simple approach for investigating the thermal behavior of many compounds and materials,[84] including the cracking kinetics of pure model compounds.[85] Figure 3-1 shows the typical weight loss and temperature curves of model compound pyrolysis in TGA experiments. Both compounds have comparable weight-loss curves, and show little change before the onset of cracking (2.3 wt% and 2.5±0.2 wt% for [Et-Py]NiTPP and 2[Et-Py]NiTPP, respectively). These small losses were likely due to the elimination of small amounts of impurities,[86] such as adsorbed solvent molecules from synthesis,[47] since no appreciable cracking is expected at such low temperatures. Furthermore, TGA confirms that these compounds do not evaporate prior to reaching the onset of cracking at ca. 350 °C and so are suitable for investigating thermal cracking reactions in the liquid phase. The weight loss observed after the onset of decomposition corresponds to cracking of the molecules and subsequent evaporation of the lighter fragments. For these compounds, the first bond that is likely to crack is the weak aliphatic C–C bond in the ethyl bridge (lowest BDE); therefore, cleavage of this bond should initiate radical chain reactions. Similar observations are reported by Lebedeva et al.,[87] whose experimental results show that cracking of the substituent alkyl groups is the first stage of decomposition of zinc(II) tetra-*tert*-butyltetraphenylporphyrin in TGA experiments.

Coke residue was observed at the end of TGA experiments at 500 °C, and the yield of coke is reported in Table 3-1. These yields were adjusted for mass

loss due to the evaporation of solvents and impurities at low temperatures. Differences in the coke yield compared to those observed by Alshareef et al.[11] for a series of archipelago compounds of similar molecular architecture can be attributed to the nature of the central aromatic group. They observed that the chemistry of the central ring system in the asphaltene model compound can have a major impact on coke formation. Moreover, the sheer size of the NiTPP aromatic core would hinder evaporation even after cleavage of the side groups, leading to a more conserved liquid phase, and hence, an increased coke yield. However, these values are not surprising, since asphaltenes typically give an MCR content or coke yield of ca. 50 wt%.[3,29,62]
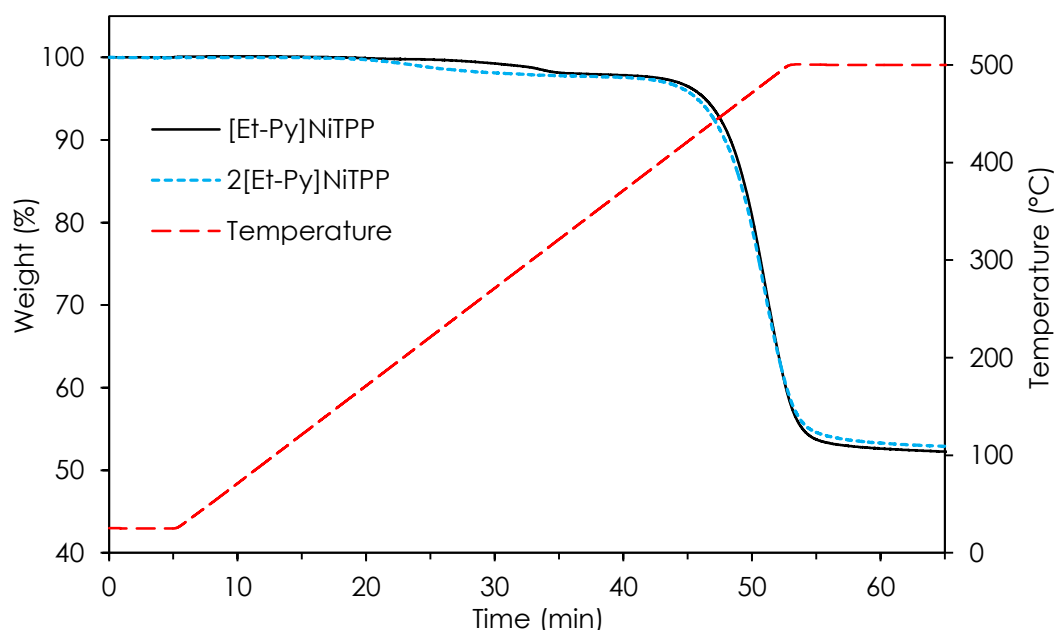
Figure 3-1. Typical weight loss and temperature curves of model compound pyrolysis in TGA experiments

The apparent Arrhenius activation energy of cracking (E_a) and pre-exponential factor (A), via first-order kinetics, were calculated using the differential method of Alshareef et al.[85] of normalized weight loss versus temperature, and can also be found in Table 3-1. At least two experiments were performed for each compound to confirm repeatability, and average values are shown. Initial cracking kinetics for the porphyrin compounds fell within the range reported by Alshareef et al.,[11] 140.6–253.1 kJ/mol, and are consistent with

cleavage of the ethano bridge. Measured kinetic parameters are also in good agreement with reported values by Poutsma[88] for liquid-phase pyrolysis of 1,2-diphenylethane (since this compound contains a $H_2C–CH_2$ bridge between two aromatic groups, it should exhibit similar cracking kinetics); E_a in the range of 201.3–279.5 kJ/mol and a log(A) of 12.7–18.4 min^{-1}.

Table 3-1. Thermogravimetric analysis (TGA) results for the model compounds

Compound	MW, g/mol	Loss before cracking, wt%	Coke yield, wt%	E_a, kJ/mol	log(A, min^{-1})
[Et-Py]NiTPP	899.7	2.3	53.4	212.9	13.86
2[Et-Py]NiTPP	1128.0	2.5±0.2	54.0±0.2	189.5±1.5	12.27±0.09
Py–[Φ]–Py ^{a}	540.7–678.9	2.9 ^{b}	3–33	140.6–253.1	9.6–18.3

^{a} Three-island archipelago compounds studied by Alshareef et al.[11] consist of two pyrenyl groups tethered by ethano bridges to a central aromatic group, [Φ]

^{b} Average weight loss before 200 °C for most of the model compounds

3.2   Phase equilibrium calculations

Due to their relatively low boiling point, the olefins (1-C$_{16}$, 1-C$_{18}$, and *trans*-stilbene) are expected to vaporize at reaction conditions. Thus, the amount of olefin loaded for microreactor experiments was selected based on calculation of vapor-liquid phase equilibrium to ensure the presence of a liquid phase. Intrinsic kinetics of elementary reactions depend on the chemical potential of the reacting species, because at equilibrium microscopic reversibility is achieved.[79] Although kinetic analyses often use concentration as an empirical substitution for more precise measures of chemical potential, for multiphase reactions the gas phase fugacity of a component is much more accessible; thus, fugacity was chosen to represent the chemical potential of the olefin, due to its presence in the vapor phase. Products obtained in thermal cracking of 1-C$_{16}$ at 410 °C for 20 min were detected by GC-FID (Figure 3-2) and GC-MS, and fall into two general categories; those with molecular weight lower than 1-C$_{16}$ (complete series of alkanes/alkenes in the C$_7$ to C$_{15}$ range, including isomeric products) and those with higher molecular weights (series of alkanes/alkenes in the C$_{17}$ to C$_{32}$ range).

Due to the low extent of cracking, addition, and homopolymerization of the olefin (Figure 3-2), changes in 1-C_{16} fugacity during reaction were deemed insignificant and within the range of error. In terms of the model compounds, they are expected to be present in the liquid phase since [Et-Py]NiTPP and 2[Et-Py]NiTPP have melting points in the range of 178–182 °C, and TGA confirmed the low volatility of the samples prior to cracking; therefore, mass concentration was used for these compounds in the kinetic expressions.
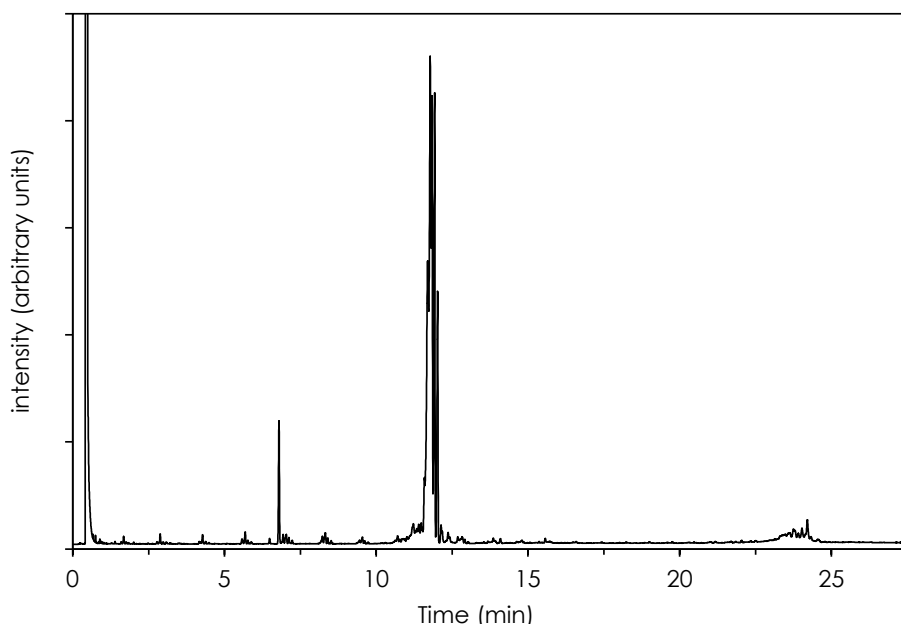
Figure 3-2. GC-FID spectrum of products from thermal cracking of 1-C_{16} at 410 °C for 20 min. Peaks at 6.80 min and 11.75 min correspond to naphthalene (internal standard) and 1-C_{16}, respectively.

The fugacity of the olefin rich vapor phase was estimated with VMGSim[89] using the Peng–Robinson cubic equation of state. To validate the calculation of the fugacities by this method, and to separate possible errors in fugacity from reaction kinetics, vapor-liquid equilibrium data for boiling point and vapor pressure for *trans*-stilbene were compared to VMGSim estimates. Figure 3-3 shows how VMGSim estimates for the vapor pressure of stilbene compare to reported literature values. Literature values for the normal boiling point of stilbene range from 306.4 to 307 °C,[90-93] versus a VMGSim estimate of 307 °C. Consequently, simulations can be deemed accurate for the simple components (*trans*-stilbene,

28

1-C_{16}, and 1-C_{18}), and suggest that the fugacity estimates are reliable. In regard to either α-olefin, it can be certain that their phase behavior will be similar, and that accurate fugacity estimates can be assigned relative to each other. Figure 3-4 shows how the calculated fugacity for 1-C_{16} varies with olefin loading, gradually increasing until enough olefin is present to maintain a liquid phase.
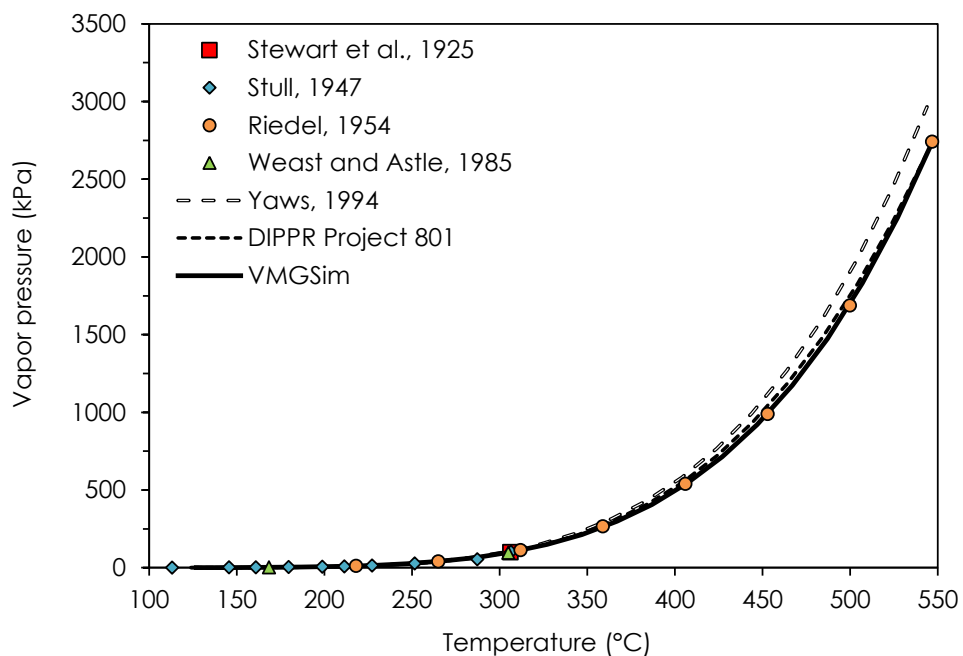
Figure 3-3. Comparison between VMGSim estimates for the vapor pressure of *trans*-stilbene and reported literature values[94-99]
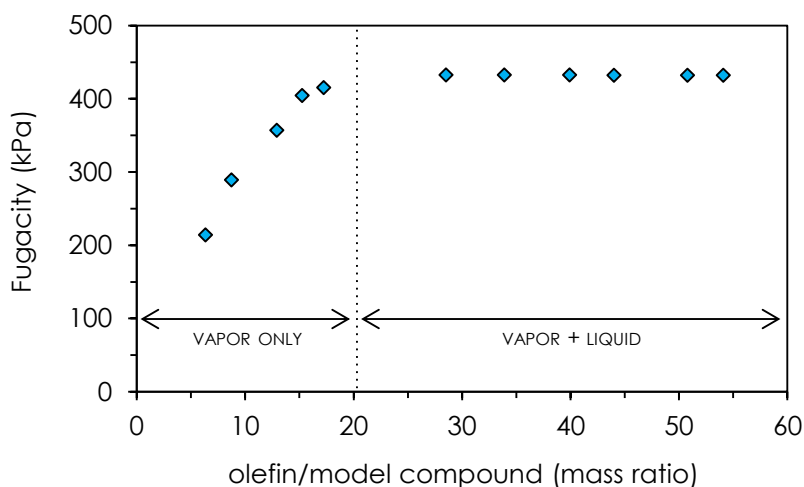
Figure 3-4. Variation of 1-hexadecene fugacity with olefin loading

3.3   Microreactor heating profile

The microreactor heating profile for thermal cracking experiments was obtained and its repeatability validated (Figure 3-5). The heat-up curve was obtained using a modified microreactor that allowed for a thermocouple to be inserted into the body of the reactor. The empty reactor was then purged with nitrogen and immersed in the fluidized sand bath, following the same procedure used for cracking experiments. The inner reactor temperature was recorded as a function of time. Although heat up of the feed and liner were not accounted for, both should have a negligible effect on the temperature profile, given their small mass in contrast to the mass of the reactor itself. For a sand bath set point of 365 °C, the temperature in the reactor was stable between 365–368 °C, and the heating and cooling times were consistent from run to run. Thus, temperature fluctuations or variations in heating/cooling times can be discounted as sources of variability from experiment to experiment.
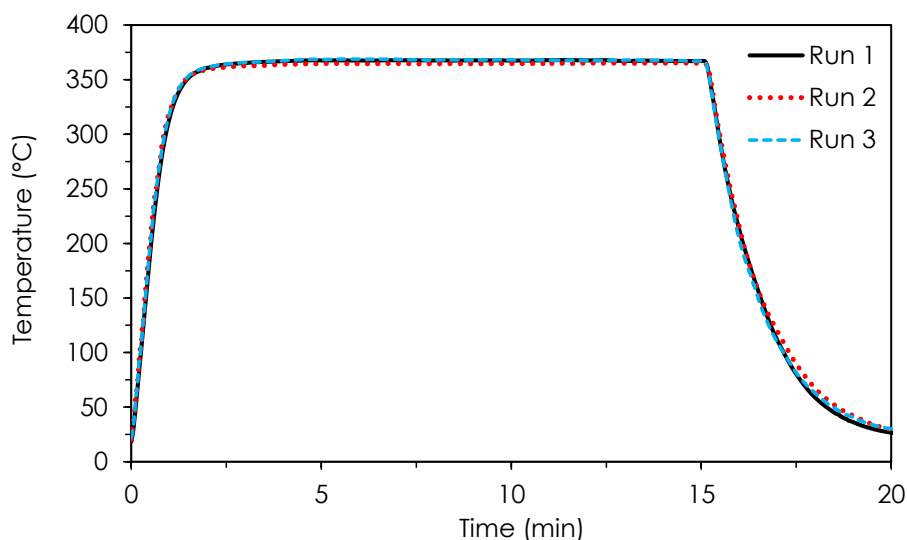
Figure 3-5. Microreactor heating profile at a sand bath set point of 365 °C for three consecutive runs shows excellent repeatability

3.4   Cracking of 2[Et-Py]NiTPP with 1-hexadecene and 1-octadecene

To verify the dependence of the main addition product on the addition reaction of the olefin in the liquid-phase cracking of the model compounds, pure 2[Et-Py]NiTPP was thermally cracked at 375 °C for 15 min, and with 1-C_{16} and 1-C_{18}

in subsequent experiments, and the reaction products analyzed by MALDI-MS. The mass spectrum of the products obtained from pyrolysis of 2[Et-Py]NiTPP with and without 1-C_{16} (Figure 3-6) shows cracked products with molecular weights lower than the parent compound and heavier species arising from addition reactions (up to ca. m/z 2500 Da). MALDI-MS analysis of 2[Et-Py]NiTPP does not contain these mass peaks with m/z greater than the parent compound, except for some impurities; therefore, these heavy ions are not instrumental artifacts.
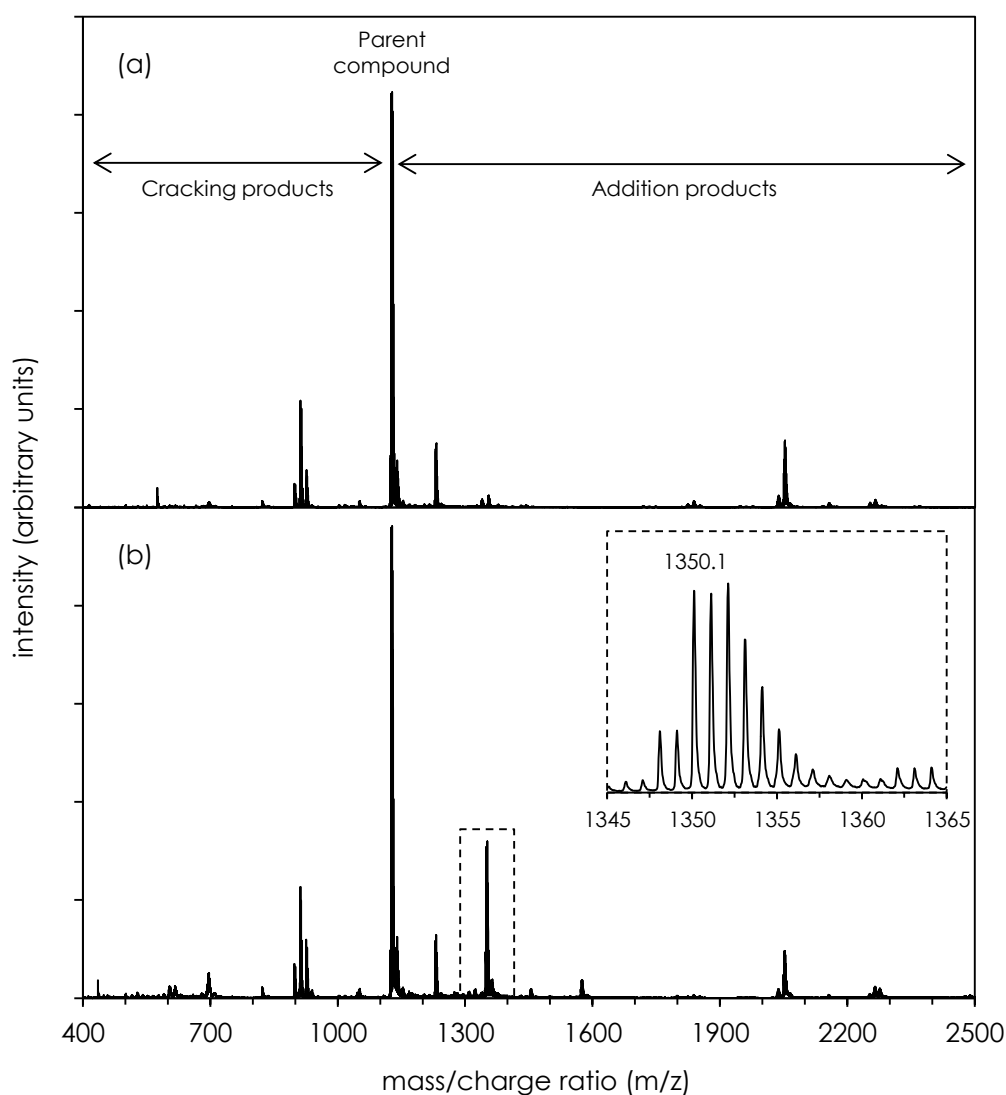
Figure 3-6. MALDI mass spectrum of products from cracking of (a) 2[Et-Py]NiTPP at 375 °C for 15 min and (b) 2[Et-Py]NiTPP with 1-C_{16} at equal conditions. Reaction with 1-C_{16} shows the formation of the coupling product at m/z 1350.1 (and corresponding isotope peaks).

Cracking with 1-C$_{16}$ shows the formation of an addition product of m/z value consistent with that of the olefin plus the model compound, and the MS/MS spectrum of the ion from the addition product at m/z = 1350.1 supports addition through the alkyl bridge (Figure 3-7). This pathway for addition has been observed by Alshareef et al.,[10] who emphasize that addition reactions occur predominantly on the alkyl chains and bridges attached to aromatic ring systems, rather than to the aryl carbons. Furthermore, in reactions with 1-C$_{18}$ the olefin addition peaks shift by 28 mass units, consistent with the 2 additional CH$_2$ in the alkyl chain (Figure 3-8). In this case, the fragmentation pattern of the precursor ion by MALDI MS/MS spectrometry is also in accordance with the proposed structure (Figure 3-9), which involves addition to the bridge. Detection by MALDI-MS spectrometry confirms addition of the olefin to the model compound; hence, the olefin-porphyrin coupling product must form at a rate higher than it is consumed by reaction, giving the strong signal of the ion due to the addition product illustrated in the mass spectra of Figures 3-6 and 3-8.
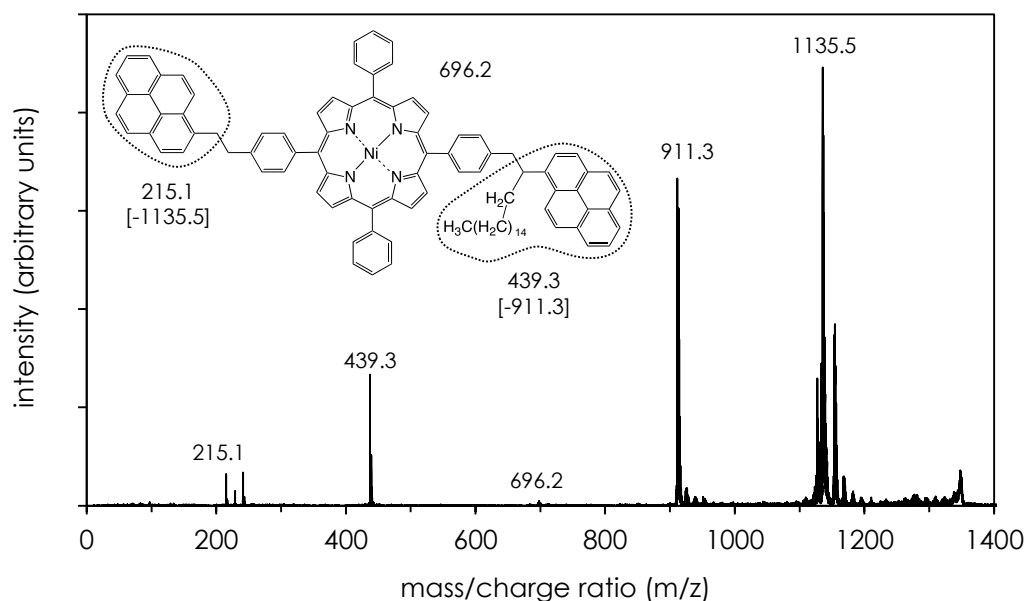
Figure 3-7. MALDI MS/MS spectrum of the m/z 1350.1 precursor ion shown in Figure 3-6b. Dashed lines indicate the cracked fragments appearing on the MS/MS spectrum, and values in brackets indicate the mass of the product molecule minus the cracked fragment. Fragmentation pattern is consistent with the drawn structure.
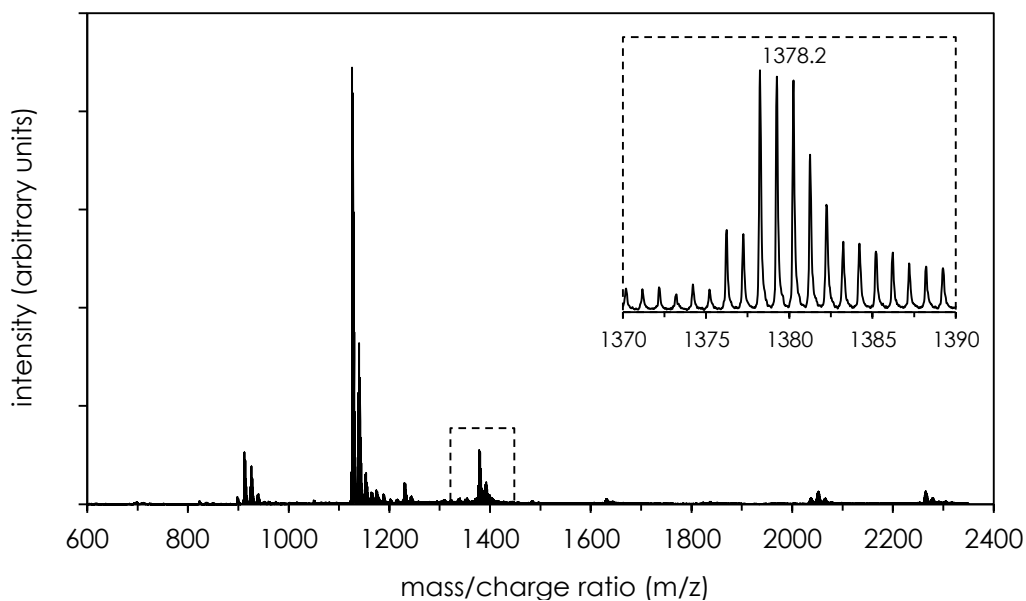
Figure 3-8. MALDI mass spectrum of products from thermal cracking of 2[Et-Py]NiTPP with 1-C$_{18}$ at 375 °C for 15 min. Spectrum shows the formation of the coupling product at m/z 1378.2 (and corresponding isotope peaks), consistent with a shift of 28 mass units from 2 additional CH$_2$ in the alkyl chain.
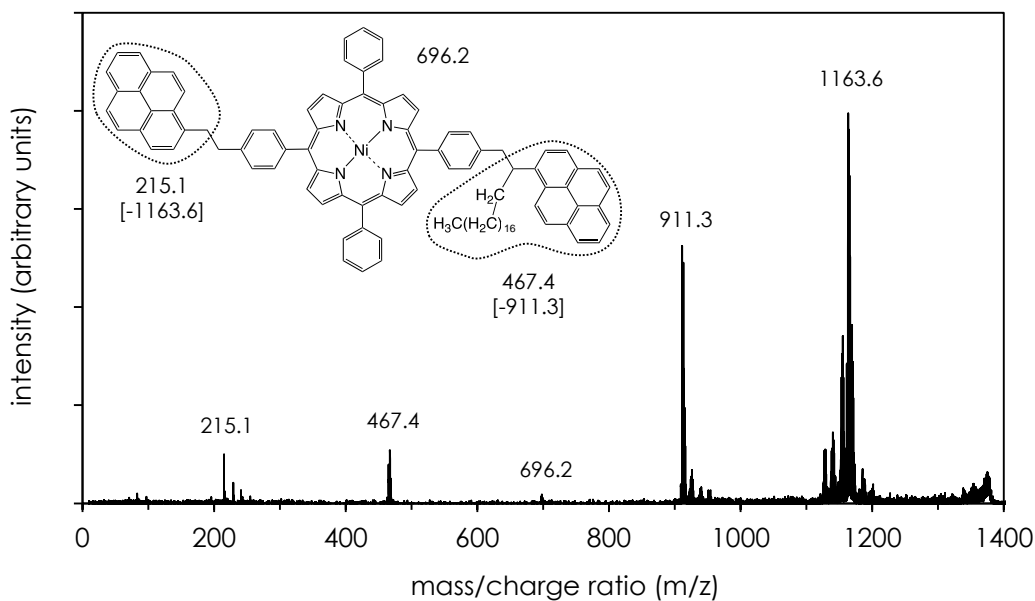
Figure 3-9. MALDI MS/MS spectrum of the m/z 1378.2 precursor ion shown in Figure 3-8. Dashed lines indicate the cracked fragments appearing on the MS/MS spectrum, and values in brackets indicate the mass of the product molecule minus the cracked fragment. Fragmentation pattern is consistent with the drawn structure.

3.5   ¹H NMR spectroscopy of reaction products

¹H NMR spectrum of the products obtained from thermal cracking of 2[Et-Py]NiTPP with 1-C$_{16}$ at 375 °C for 15 min shows no significant change in the aromatic region (Figure 3-10), excluding the possibility of substitution on the aromatic rings. New resonances arising at δ 5.45 do not provide a definite location for bridge formation, but simulation of the ¹H NMR spectra of addition products using MestReNova software also eliminates addition through aromatic carbons. Consequently, ¹H NMR spectra are consistent with addition through the ethano bridge between the aromatic ring groups, consistent with MALDI MS/MS spectrometry results and previous pyrolysis studies of pyrene-based archipelago model compounds,[10] which show that these pyrene-based bridged structures undergo addition through the attached alkyl groups. In this case, however, comparison of the experimentally measured ¹H NMR spectra and the calculated or simulated spectra using MestReNova did not allow assignment of a specific preferred product structure.
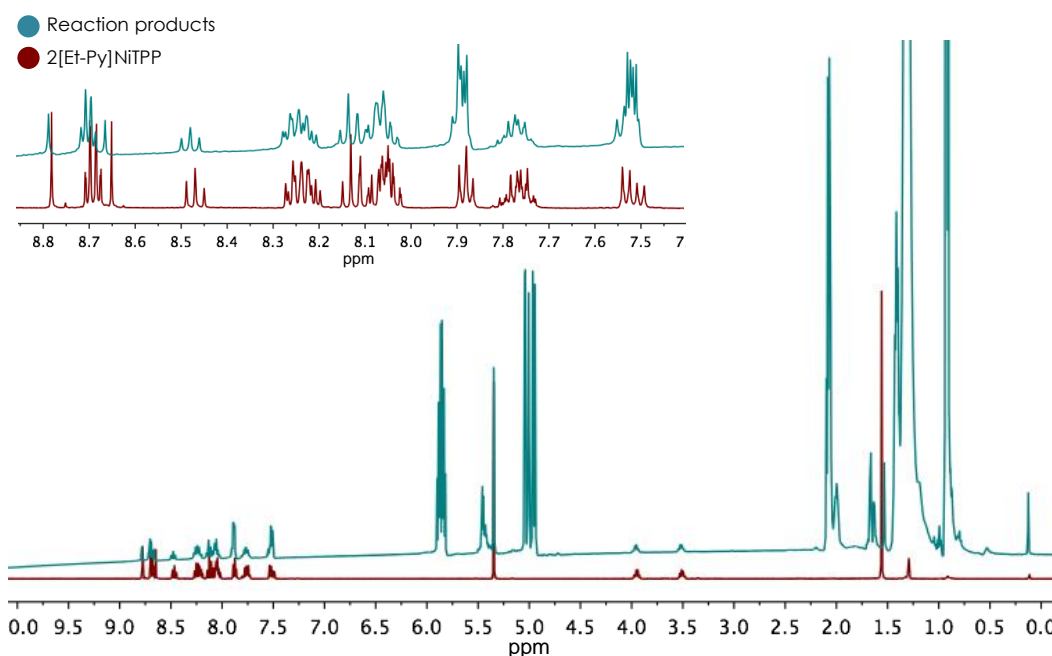
Figure 3-10. ¹H NMR (500 MHz) spectrum of products from pyrolysis of 2[Et-Py]NiTPP with 1-C$_{16}$ at 375 °C for 15 min. The aromatic region is enlarged.

3.6   Cracking of [Et-Py]NiTPP with 1-hexadecene

Thermal cracking reactions at different times and temperatures of [Et-Py]NiTPP with 1-C_{16} allowed a more detailed kinetic analysis. Conversion of [Et-Py]NiTPP at 375 °C as a function of time in reactions with 1-C_{16} is shown in Figure 3-11. The data point at 20 min is the average value from 5 separate reactions, and error bars correspond to the standard deviation. Replicates and statistical checks (test for outliers for the small data sets – Grubbs' T-test) were used to remove two data sets that, for unclear reasons, were clearly outliers. The concentration-time data indicate first-order reaction in model compound concentration, with a rate constant for [Et-Py]NiTPP conversion of (1.9 ± 0.1) x 10^{-4} s^{-1}, calculated from fitting data to a first-order kinetic model for a batch reactor:

$$X = 1 - \exp(-k \times t) \tag{3-1}$$

where X (%) is conversion, k (s^{-1}) is the rate constant, and t (s) is time.
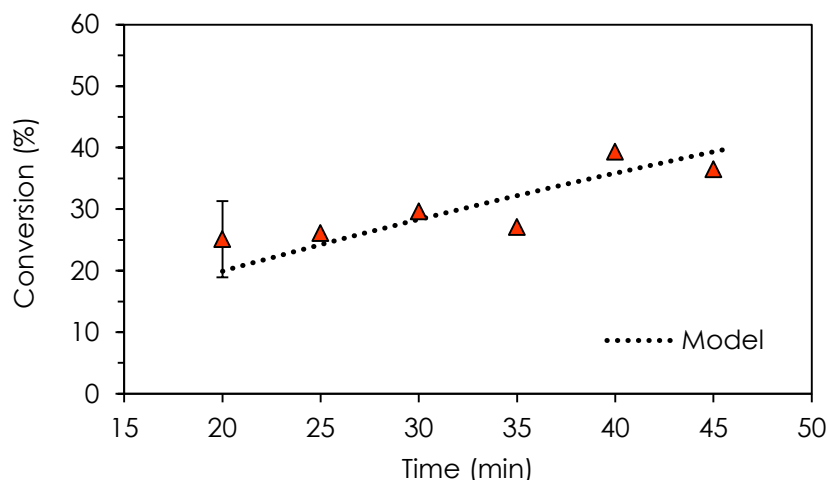
Figure 3-11. Conversion of [Et-Py]NiTPP at 375 °C as a function of time in reactions with 1-C_{16}. Model is based on first-order kinetics in model compound concentration, with a rate constant of (1.9 ± 0.1) x 10^{-4} s^{-1}.

This model fits over a range of conversion and is in good agreement with experimental values, which show a fairly linear trend within the error of the data based on the initial condition. In reactions with 1-C_{16}, an increase in the conversion of [Et-Py]NiTPP can be observed relative to cracking of the pure model compound; for example, 13.3% conversion in reactions with no added

35

olefin (375 °C, 20 min). Since the porphyrin is the main radical generator during cracking, it is likely that these unsaturated species act as radical scavengers, reacting with the parent radicals that could otherwise re-stabilize, for example, via hydrogen abstraction. Thus, the olefin addition reaction would contribute to an increase in the rate of disappearance of the parent compound, as more pathways for reaction are added, causing an increase in conversion.

Two additional time series were performed at 390 °C and 410 °C, and the corresponding rate constants were obtained. The temperature dependence of the rate constants can be well described by the Arrhenius equation:

$$k = A \exp\left(\frac{-E_a}{RT}\right)$$

(3-2)

where E_a (kJ/mol) is the apparent activation energy, A (s^{-1}) is the pre-exponential factor, R (kJ mol^{-1} K^{-1}) is the universal gas constant, and T (K) is temperature. The Arrhenius plot of first-order rate constants for overall conversion of [Et-Py]NiTPP in reactions with 1-C_{16} is presented in Figure 3-12.
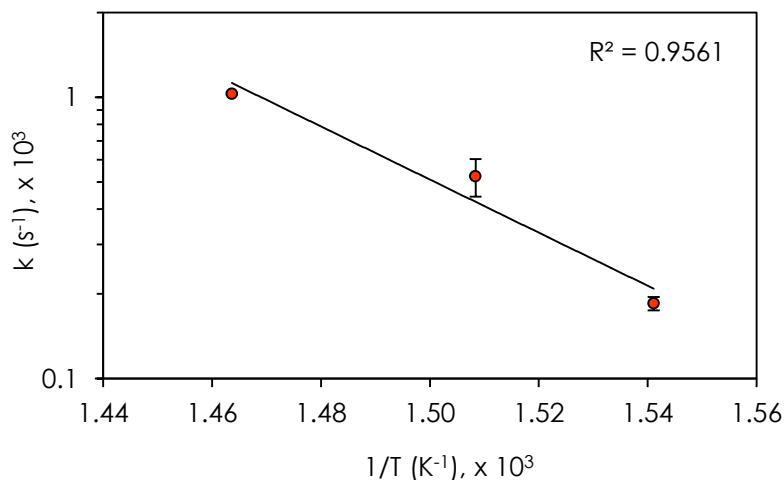
Figure 3-12. Arrhenius plot of first-order rate constants for conversion of [Et-Py]NiTPP in thermal cracking reactions with 1-C_{16}

The reaction is relatively slow, but is accelerated considerably with temperature. The estimated activation energy of 180.6 ± 38.7 kJ/mol is consistent with a mechanism dominated by free-radical chain reactions, where the

propagation steps are significant, and is comparable with available literature data. For example, Smith and Savage[70] report an apparent activation energy of 167 ± 25 kJ/mol for pyrolysis of 1,3-bis(1-pyrene)propane, while Savage et al.[100] report a value of 170.7 kJ/mol for cracking of 1-dodecylpyrene. An estimate of log(A) equal to 10.9 ± 3.0 s^{-1} was obtained from the Arrhenius plot (Figure 3-12).

Lastly, Figure 3-13 and Figure 3-14 show how the experimental data compare to the first-order kinetic model using the calculated apparent Arrhenius parameters to estimate rate constants and conversion, in reactions with 1-C$_{16}$ at 375 °C for different times (Figure 3-13), and in reactions with the olefin for 20 min over a range of temperatures (Figure 3-14).
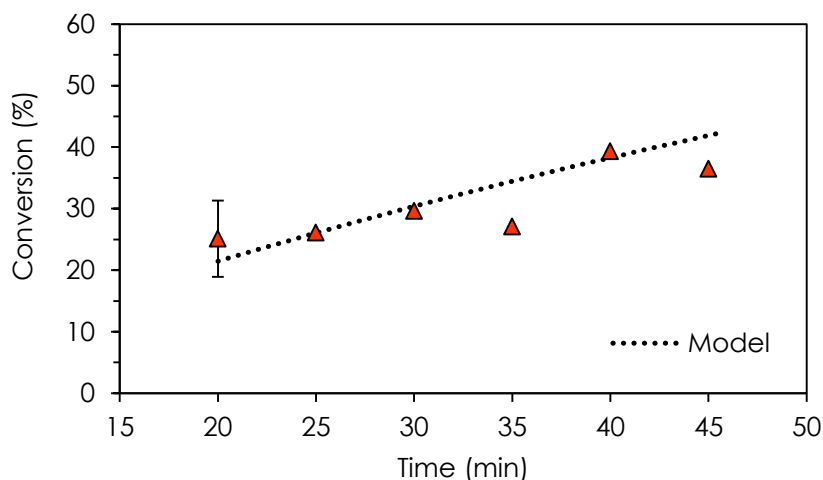
Figure 3-13. Conversion of [Et-Py]NiTPP at 375 °C as a function of time in reactions with 1-C$_{16}$. Model is based on first-order kinetics in model compound concentration, with an E$_a$ of 180.6 ± 38.7 kJ/mol and log(A) of 10.9 ± 3.0 s^{-1}.
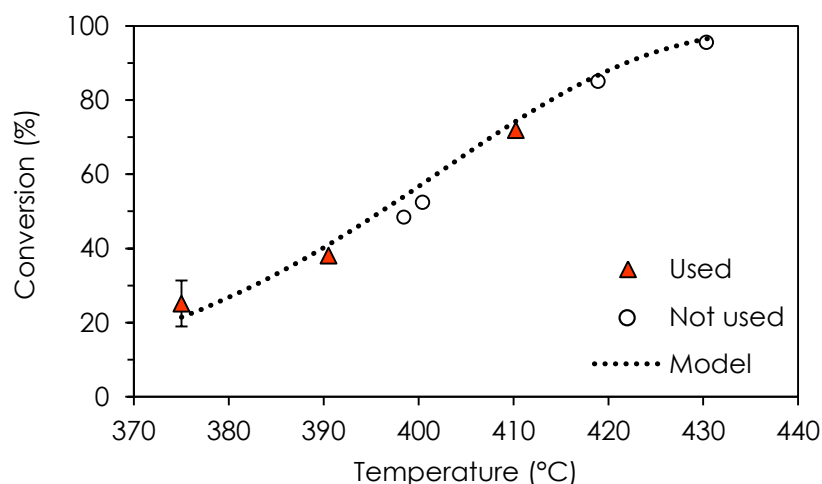
Figure 3-14. Conversion of [Et-Py]NiTPP as a function of temperature in reactions with 1-C$_{16}$ for 20 min. Model is based on first-order kinetics in model compound concentration, with an E$_a$ of 180.6 ± 38.7 kJ/mol and log(A) of 10.9 ± 3.0 s^{-1}. Circles indicate data points that were not used in estimating the kinetic parameters.

The molar yield for the olefin-[Et-Py]NiTPP addition product, defined as the number of moles of product formed from the decomposition of 100 moles of the parent model compound in the microreactor experiments, is shown in Figure 3-15 as a function of temperature. A combination of the data from HPLC and MALDI-MS were used to calculate the yield of addition product. Only peaks above the noise level of the spectrum were included. A sample calculation can be found in Appendix B. The data suggest that the coupling product is an intermediate that is subject to formation and destruction, consistent with observations by Alshareef et al.[10,11] They indicated that addition products formed at low conversions remain reactive, and would thus continue to react to give smaller cracked fragments and still larger structures as conversion increases. In this sense, the resulting coupling product from the olefin-porphyrin addition will likely participate in further free-radical reactions, such as hydrogen abstraction to produce a radical, which can rearrange to a more stable radical, combine with another radical, undergo cracking via β-scission, or add to another olefin, amongst other possibilities. Ultimately, these intermediate species are bound to undergo changes over time, reacting to form lower and higher molecular weight species.
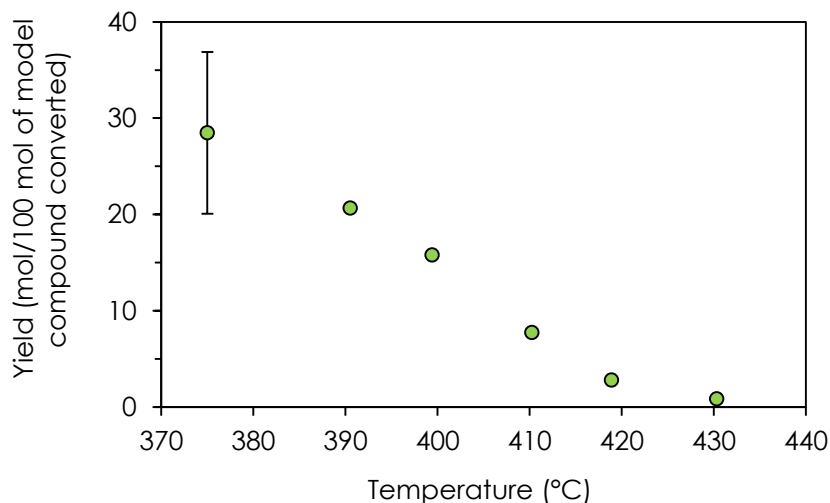
Figure 3-15. Yield of the coupling product in reactions of [Et-Py]NiTPP with 1-C_{16} as a function of temperature (reaction time: 20 min)

For the olefin-porphyrin coupling product, C, the following rate expression can be derived:

$$\frac{d[C]}{dt} = k_1 f_o[\dot{P}] - k_2[C]$$

(3-3)

where [C] (mg/cm³) is the addition product mass concentration, k_1 (s⁻¹ kPa⁻¹) is the rate constant for the parent radical-olefin addition step, f_o (kPa) is the olefin fugacity, $[\dot{P}]$ (mg/cm³) is the parent radical concentration, and k_2 (s⁻¹ kPa⁻¹) is the rate constant for consumption of the addition product. Assuming that $[\dot{P}]=\beta(T).[P]$, so that the parent radical concentration is proportional to the amount of remaining parent compound, [P], at a given T. In this expression, the temperature dependence of β depends on the underlying elementary reactions and their activation energies. This result gives:

$$\frac{d[C]}{dt} = k_1 \beta f_o[P] - k_2[C]$$

(3-4)

where k_1, β, and k_2 are all functions of temperature. Additionally, from the kinetics derived for model compound conversion in reaction with 1-C_{16}:

$$\frac{d[P]}{dt} = -k[P]$$

(3-5)

where k (s^{-1}) is defined by the following Arrhenius parameters: E_a of 180.6 ± 38.7 kJ/mol and log(A) of 10.9 ± 3.0 s^{-1} (as previously estimated). Solving these two differential equations gives (for a set temperature, k_1, β, and k_2 constant):

$$[C] = \frac{k_1 \beta f_o [P]_o}{k_2 - k} \left[e^{-kt} - e^{-k_2 t} \right]$$

(3-6)

where $[P]_o$ is the concentration of the parent compound at t = 0. Fitting this model to the experimental yield of addition product at 375 °C (Figure 3-16) by minimizing the total sum of squares gives the following estimates for the rate constants: k = 2 x 10^{-4} s^{-1}, k_1 β = 5.1 x 10^{-7} s^{-1} kPa^{-1}, and k_2 = 2 x 10^{-3} s^{-1}. These rate estimates suggest that the addition product is consumed at a rate faster than the parent compound (k_2 > k by an order of magnitude), indicating that these alkylated adduct structures react even more readily than the parent compounds. Likewise, further cracking of these alkylated adduct structures, for example, via cleavage of the H_2C–CH_2 bridge between the aromatic groups, would generate a more stable secondary benzylic radical, which in turn is a more favorable reaction intermediate. This observation also suggests that the adduct structures are more reactive, which is consistent with the estimated rates.
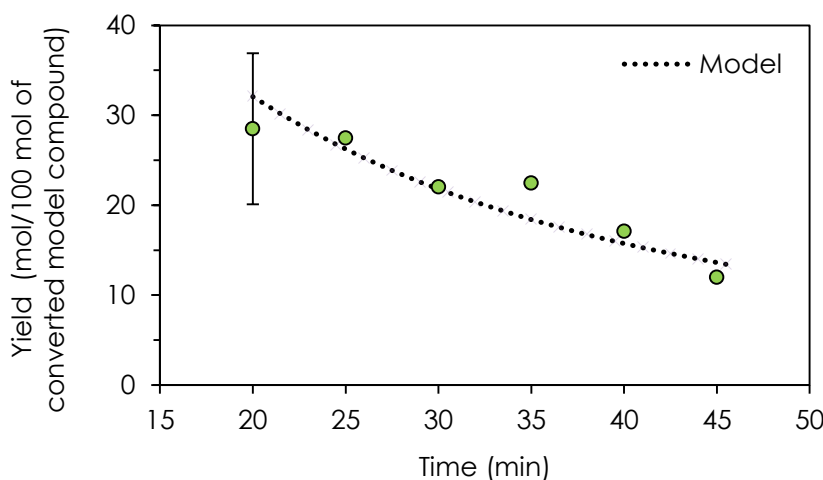
Figure 3-16. Yield of the coupling product in reactions of [Et-Py]NiTPP with 1-C_{16} as a function of time (reaction temperature: 375 °C). Model follows Equation (3-6), with the rate constants k = 2 x 10^{-4} s^{-1}, k_1 β = 5.1 x 10^{-7} s^{-1} kPa^{-1}, and k_2 = 2 x 10^{-3} s^{-1}.

3.7   Rate-determining step

Figure 3-17 illustrates the two elementary steps required to form the olefin-porphyrin addition product: olefin addition to the parent radical and subsequent hydrogen abstraction that forms the stable addition product. Estimates of the Arrhenius parameters and rate constant for both reactions are listed in Table 3-2. Activation energies and pre-exponential factors are averaged from values given by Freund and Olmstead,[101] Smith and Savage,[70-72] Khorasheh and Gray,[57] and Fischer and Radom,[69] and are listed in Table 1-2. Although these rate parameters were obtained for compounds of lower molecular complexity, they can still be used to reach a robust conclusion on the kinetics of these reactions, considering they are both second order reactions. Olefin addition to the parent radical is significantly slower than the subsequent hydrogen abstraction (reaction rate estimate for addition is smaller by an order of magnitude), based on literature comparisons. This observation is consistent with the expected behavior, considering the significant amount of available abstractable hydrogen, both benzylic and aliphatic. In turn, the addition reaction between the olefin and the parent radical requires that these two species collide with sufficient energy and in the correct orientation. Taking these factors into account, addition of the olefin to the parent radical is likely rate-limiting, so that the intermediate radical formed stabilizes rapidly via hydrogen abstraction.
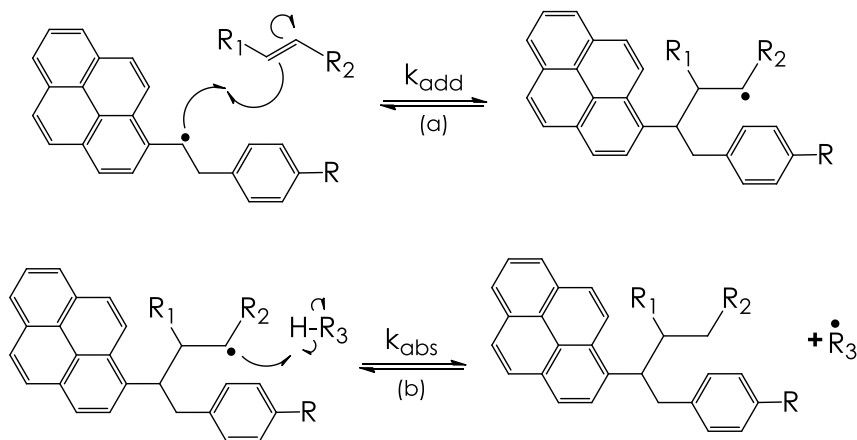
Figure 3-17. Elementary steps involved in the formation of the coupling product: (a) radical addition to the unsaturated bond and (b) hydrogen abstraction

Table 3-2. Arrhenius parameters and reaction rate estimates at 400 °C for the elementary steps involved in the formation of the coupling product

Step	E_a, kJ/mol	log(A, L mol^{-1} s^{-1})	k, L mol^{-1} s^{-1}	
(a) Addition	33.5	7.36	k_{add}	5.8×10^4
(b) H-abs	29.3	8.00	k_{abs}	5.3×10^5

3.8 Olefin reactivity

In addition to 1-C$_{16}$, thermal cracking experiments with 1-C$_{18}$ and *trans*-stilbene were carried out to investigate the impact of α-olefin chain length and double bond conjugation on the addition reaction of the olefin in the liquid phase. Table 3-3 shows the impact of the added olefin on the yield of the coupling product in thermal cracking reactions with the model compound at 375 and 400 °C for 20 min. At least two experiments were performed with each olefin to confirm repeatability, and average values are shown.

Table 3-3. Impact of the added olefin on the yield of the coupling product in thermal cracking reactions with [Et-Py]NiTPP (reaction time: 20 min)

Olefin	Conversion, wt%		Yield, mol/100 mol of converted model compound		Olefin fugacity, kPa	
	375 °C	400 °C	375 °C	400 °C	375 °C	400 °C
1-C$_{16}$	25.1±6.2	50.5	28.5±8.4	15.8	432	583
1-C$_{18}$	21.9	44.9	29.0	14.5	277	387
trans-stilbene	23.9	40.7	18.2	3.4	308	434

According to the data in Table 3-3, formation of the addition product is less favored in reactions with *trans*-stilbene. The difference in the yield between *trans*-stilbene and the α-olefins is statistically significant, outside the range of experimental error and uncertainty in the calculated fugacity. Consequently, the rate constant for addition of *trans*-stilbene is much lower. This result suggests that some other factor, aside from fugacity of the olefin reactant, must affect the main reaction pathway for radical addition to the unsaturated bond. Normally,

the preferred pathway for free-radical reactions is dominated by the stability of the parent radical, the stability of the intermediate radical addition product, or the reactivity of the reactants. In this case, the most stable radical species is adjacent to the pyrene due to delocalization of the unpaired electron over the π orbital system,[102] so that the most favorable parent radical for all the reactions listed in Table 3-3 is that shown in Figure 3-18. Consequently, unsaturated species probably add next to the pyrene, forming a family of addition products all in the same location. As discussed above, the exact position between the two carbons in the bridge is difficult to establish from MALDI MS/MS and ^{1}H NMR spectra data.
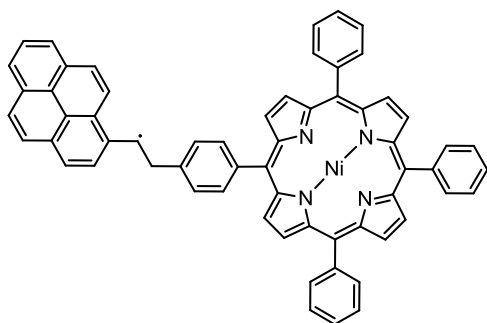
Figure 3-18. Most favorable radical from [Et-Py]NiTPP

The stability of the intermediate radical addition product must take into account the fact that addition of the radical to the π-bond of the olefin is regioselective,[103] giving the more stable carbon radical as an intermediate. Thus, the addition reaction causes the radical to move away from the pyrene, resulting in a secondary alkyl radical with either α-olefin, and a more stable benzylic radical with *trans*-stilbene (Figure 3-19). The added stability of the benzylic radical is primarily due to the delocalization resonance effect, as noted by Fischer and Radom,[69] who report that benzyl radicals reacted 100–400 times more slowly than methyl in addition reactions to alkenes, and that much of this difference could be the result of the radical stabilizing effect of the phenyl group. Therefore, if the stability of the intermediate radical controlled the rate of formation of the addition product, higher yields would be expected in reactions with stilbene. However, the experimental data indicates that stilbene is less reactive under the same conditions and similar fugacities, which suggests that the reactivity of the reactants must have a greater impact on the outcome.
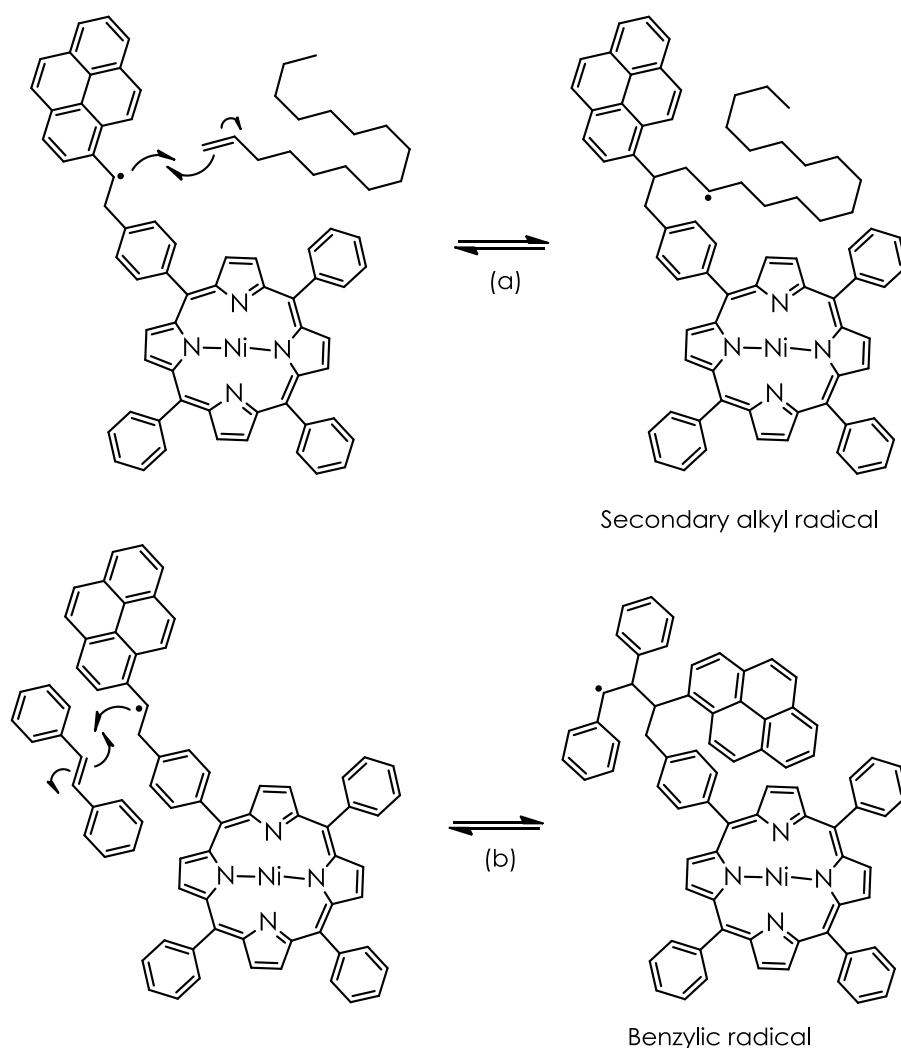
Figure 3-19. Addition of the parent radical to the unsaturated bond of
(a) 1-hexadecene and (b) *trans*-stilbene

According to the literature, two important factors influence the reactivity of olefins in addition reactions with radicals: the electron density on the double bond and steric hindrance effects. A lower electron density in the double bond of stilbene due to delocalization of the electrons from conjugation, would lower its reactivity towards radical addition,[104,105] compared to α-olefins with localized π-electrons. The nature of the substituents on the olefinic bond has been noted to affect the rate of addition of radicals, as these influence the interactions between the singly occupied orbital of the radical (SOMO) and the lowest unoccupied orbital (LUMO) and/or the highest occupied orbital (HOMO) of the π-

C–C bond.[106,107] Likewise, substituents on the alkene could sterically hinder addition to radicals and affect the rates of addition,[108,109] as in the present case, where stilbene has bulkier phenyl substituents on the double bond, compared to the linear alkyl α-olefins. The difference in reactivity of stilbene is consistent with a combination of these factors, both electron density and steric hindrance effects. For example, Cameron and Grassie[110] report that in polymerization reactions with styrene and *trans*-stilbene, the reactivity of styrene towards radical addition was much higher than that of *trans*-stilbene, and showed that stacking of additional benzene rings onto the double bond lowered the reactivity of the olefin.

Contrary to reactions with the α-olefins, the major addition product in reactions with stilbene was m/z 1594.4. The suggested structure of this compound is presented in Figure 3-20, and is in agreement with both the experimental observations of Alshareef et al.[10] from the liquid-phase cracking of alkyl-bridged pyrene compounds such as 1,3-bis(2-pyren-1-yl-ethyl)-benzene, and with tandem MALDI MS/MS spectrometry data, as shown in Figure 3-21. The formation of this product is consistent with a mechanism involving addition of fragments of the original molecule to unsaturated bonds formed adjacent to the aromatic rings via successive hydrogen abstractions mediated by free radicals.[4,73] The result is that addition of cracked fragments to the ethano bridge is more facile than the reaction with stilbene, i.e., stilbene appears to be less reactive than any unsaturated intermediate forming during cracking of the parent compound itself.
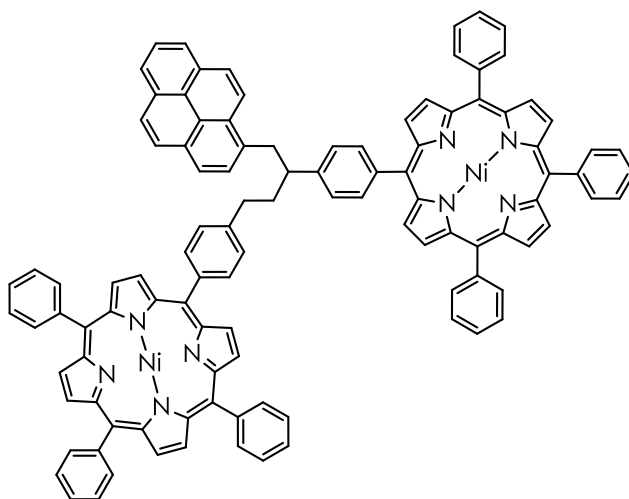
Figure 3-20. Suggested structure for the major addition product from cracking reactions of [Et-Py]NiTPP with *trans*-stilbene (m/z 1594.4)

These observations imply that the larger olefins can be quite reactive, which would indicate a way of explaining the 1-octadecene data from Table 3-3. The yield from 1-C_{18}, as compared to 1-C_{16}, is much larger than the difference in fugacity between the two olefins, so that the reaction rate constant for 1-C_{18} is larger than 1-C_{16} at the same fugacity. One possible explanation is that supramolecular interactions[23] could enhance the rates of addition. Alshareef et al.[11,20] suggest that intermolecular associative forces influence coke formation, and by extension, those reactions that give rise to coke, so that contributions to these interactions could contribute to higher addition rates. A recommendation for future studies is to investigate the reactivity of ethenyl-pyrene and other propenyl and ethenyl aromatics, since these types of olefins are much more relevant to the reactions that would be expected in upgrading of heavy bitumen fractions.
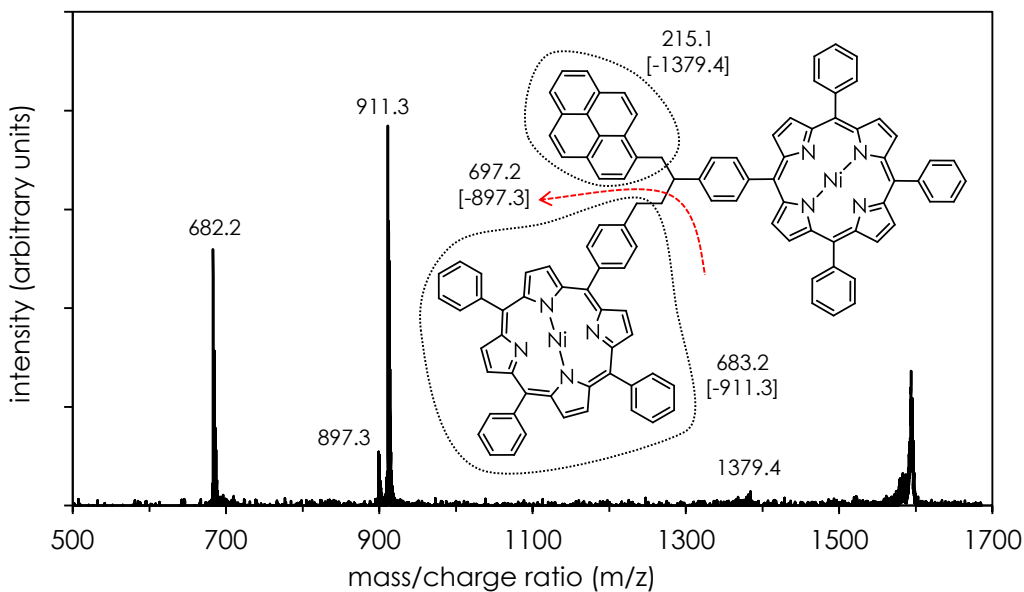
Figure 3-21. MALDI MS/MS of the m/z 1594.4 compound shown in Figure 3-20. Dashed lines indicate the cracked fragments appearing on the MS/MS spectrum, and values in brackets indicate the mass of the product molecule minus the cracked fragment. Fragmentation pattern is consistent with the drawn structure.

3.9   Implications

Present study expands on previous work by Alshareef et al., unambiguously proving the reaction pathway for olefin addition. These addition products are able to abstract hydrogen to give detectable products faster than they decompose; nevertheless, further rearrangements are expected to occur. To help illustrate this, a simplified reaction pathway showing the transition from reactants to more graphitic coke is presented in Figure 3-22. This schematic highlights the free-radical addition step as the first rate-limiting step, and that further polymerization could lead to phase separation and coke formation. Clearly, suppression of addition reactions would decrease the yield of coke during thermal cracking operations, and so the effective removal of olefins would eliminate a pathway for addition. Figure 3-22 also indicates some of the viable options for interrupting this polymerization pathway, which include reactions with hydrogen donor solvents,[111-113] catalytic hydrogenation of the generated olefins and partial hydrogenation of PAHs to give hydrogen donors,[4,114] and the removal of cracked fragments from the reacting liquid pool.

1st rate-limiting step

H-donor solvents
Catalytic hydrogenation
Removal of cracked fragments

**Phase separation and
coke formation**
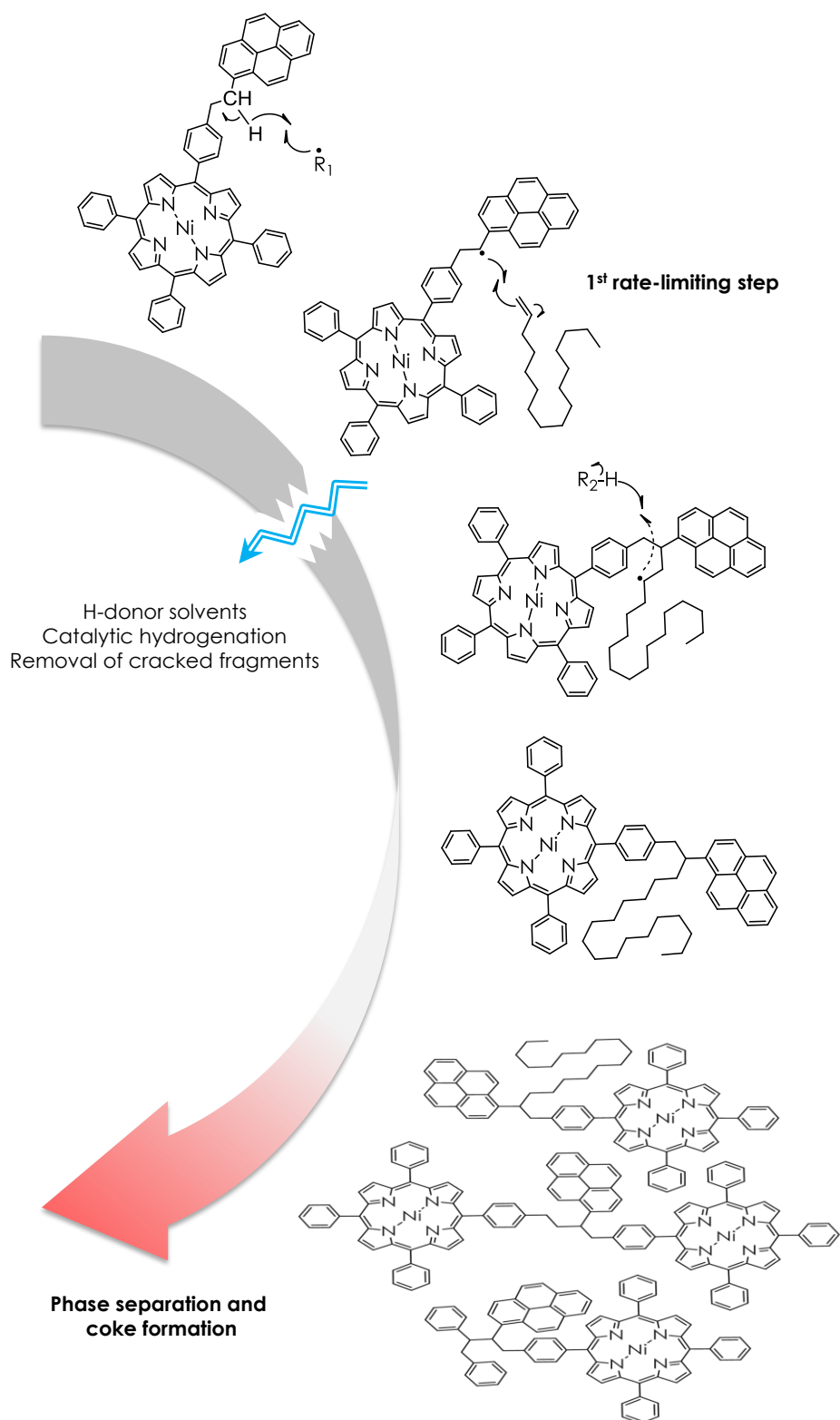
Figure 3-22. Simplified reaction pathway showing the transition from reactants to more graphitic coke. Free-radical addition step is shown as the first rate-limiting step. Further polymerization could lead to phase separation and coke formation.

CHAPTER 4:

Conclusions and Recommendations

4.1 Conclusions

Based on the thermal cracking reactions and kinetic analysis carried out in the present study, the following conclusions can be drawn regarding addition reactions of olefins to asphaltene model compounds:

- MALDI-MS spectrometry shows the formation of an addition product of molecular weight consistent with that of the olefin plus the model compound, and MS/MS and ^{1}H NMR spectra are consistent with addition to the alkyl bridge

- Kinetic data indicate first-order reaction in parent compound concentration, with energetics consistent with a free-radical chain mechanism

- Addition of the olefin to the parent radical is likely rate-limiting, so that the intermediate radical formed stabilizes rapidly via hydrogen abstraction

- Lower reactivity of *trans*-stilbene in free-radical addition is consistent with a combination of electron density and steric hindrance effects

4.2 Recommendations

Future work should investigate the reactivity of ethenyl-pyrene and other propenyl and ethenyl aromatics, since these types of olefins are much more relevant to the reactions that would be expected in upgrading of heavy bitumen fractions. Likewise, further studies should also investigate the reactivity, reaction

pathways, and structures of the reaction products of more complex asphaltene model compounds; for example, asymmetric molecules with variable lengths of the bridges, with different functional groups and aromatic cores.

REFERENCES

1. Zhao, H.; Cao, Y.; Sit, S. P.; Lineberry, Q.; Pan, W. Thermal characteristics of bitumen pyrolysis. *Journal of Thermal Analysis and Calorimetry* **2012**, *107*, 541-547.

2. Jimenez-Mateos, J.; Quintero, L. C.; Rial, C. Characterization of petroleum bitumens and their fractions by thermogravimetric analysis and differential scanning calorimetry. *Fuel* **1996**, *75*, 1691-1700.

3. Speight, J. G., Ed.; In *The Chemistry and Technology of Petroleum*; CRC Press: Boca Raton, FL, 2007.

4. Gray, M. R.; McCaffrey, W. C. Role of chain reactions and olefin formation in cracking, hydroconversion, and coking of petroleum and bitumen fractions. *Energy and Fuels* **2002**, *16*, 756-766.

5. Rakotondradany, F.; Fenniri, H.; Rahimi, P.; Gawrys, K. L.; Kilpatrick, P. K.; Gray, M. R. Hexabenzocoronene model compounds for asphaltene fractions: Synthesis characterization. *Energy Fuels* **2006**, *20*, 2439-2447.

6. Tan, X.; Fenniri, H.; Gray, M. R. Pyrene derivatives of 2,2-bipyridine as models for asphaltenes: Synthesis, characterization, and supramolecular organization. *Energy Fuels* **2008**, *22*, 715-720.

7. Sabbah, H.; Morrow, A. L.; Pomerantz, A. E.; Mullins, O. C.; Tan, X.; Gray, M. R.; Azyat, K.; Tykwinski, R. R.; Zare, R. N. Comparing laser desorption/Laser ionization mass spectra of asphaltenes and model compounds. *Energy Fuels* **2010**, *24*, 3589-3594.

8. Scherer, A.; Hampel, F.; Gray, M. R.; Stryker, J. M.; Tykwinski, R. R. Incorporation of steroidal biomarkers into petroleum model compounds. *Journal of Physical Organic Chemistry* **2012**, *25*, 597-606.

9. Schulze, M.; Scherer, A.; Hampel, F.; Gray, M.; Tykwinski, R. *Heavy porphyrins as petroleum model compounds.* Poster session presented at the 14th International Conference on Petroleum Phase Behavior and Fouling, Rueil-Malmaison, France. **2013, June**.

10. Alshareef, A. H.; Scherer, A.; Tan, X.; Azyat, K.; Stryker, J. M.; Tykwinski, R. R.; Gray, M. R. Formation of archipelago structures during thermal cracking implicates a chemical mechanism for the formation of petroleum asphaltenes. *Energy Fuels* **2011**, *25*, 2130-2136.

11. Alshareef, A. H.; Scherer, A.; Tan, X.; Azyat, K.; Stryker, J. M.; Tykwinski, R. R.; Gray, M. R. Effect of chemical structure on the cracking and coking of archipelago model compounds representative of asphaltenes. *Energy Fuels* **2012**, *26*, 1828-1843.

12. Alshareef, A. H.; Scherer, A.; Stryker, J. M.; Tykwinski, R. R.; Gray, M. R. Thermal cracking of substituted cholestane-benzoquinoline asphaltene model compounds. *Energy Fuels* **2012**, *26*, 3592-3603.

13. Soleimanisalim, A.; Gray, M. R.; Stryker, J. M.; Tykwinski, R. R. *Addition reactions of model compounds of asphaltenes during thermal cracking.* Poster session presented at the 2012 Oilsands conference, University of Alberta, Edmonton, AB, Canada. **2012, August**.

14. Akbarzadeh, K.; Bressler, D. C.; Wang, J.; Gawrys, K. L.; Gray, M. R.; Kilpatrick, P. K.; Yarranton, H. W. Association behavior of pyrene compounds as models for asphaltenes. *Energy Fuels* **2005**, *19*, 1268-1271.

15. Tan, X.; Fenniri, H.; Gray, M. R. Water enhances the aggregation of model asphaltenes in solution via hydrogen bonding. *Energy Fuels* **2009**, *23*, 3687-3693.

16. Yin, C.; Tan, X.; Mullen, K.; Stryker, J. M.; Gray, M. R. Associative π−π interactions of condensed aromatic compounds with vanadyl or nickel porphyrin complexes are not observed in the organic phase. *Energy Fuels* **2008**, *22*, 2465-2469.

17. Da Costa, L. M.; Stoyanov, S. R.; Gusarov, S.; Tan, X.; Gray, M. R.; Stryker, J. M.; Tykwinski, R.; Carneiro, D. M.; Seidl, P. R.; Kovalenko, A. Density functional theory investigation of the contributions of π−π stacking and hydrogen-bonding interactions to the aggregation of model asphaltene compounds. *Energy Fuels* **2012**, *26*, 2727-2735.

18. Soleimanisalim, A.; Tan, X.; Gray, M.; Stryker, J.; Tykwinski, R. *Investigation of aggregation of model compounds of asphaltenes in organic solutions with 1H NMR spectroscopy*. Poster session presented at the 13th International Conference on Petroleum Phase Behavior and Fouling, St. Petersburg Beach, FL. **2012, June**.

19. Rueda-Velasquez, R.; Freund, H.; Qian, K.; Olmstead, W. N.; Gray, M. R. Characterization of asphaltene building blocks by cracking under favorable hydrogenation conditions. *Energy Fuels* **2013**, *27*, 1817-1829.

20. Alshareef, A. H. Thermal cracking reactions of model compounds of asphaltenes, University of Alberta, Edmonton, 2012.

21. Pelet, R.; Behar, F.; Monin, J. C. Resins and asphaltenes in the generation and migration of petroleum. *Org. Geochem.* **1986**, *10*, 481-498.

22. Sheremata, J. M.; Gray, M. R.; Dettman, H. D.; McCaffrey, W. C. Quantitative molecular representation and sequential optimization of Athabasca asphaltenes. *Energy Fuels* **2004**, *18*, 1377-1384.

23. Gray, M. R.; Tykwinski, R. R.; Stryker, J. M.; Tan, X. Supramolecular assembly model for aggregation of petroleum asphaltenes. *Energy Fuels* **2011**, *25*, 3125-3134.

24. Groenzin, H.; Mullins, O. C. Molecular Size and Structure of Asphaltenes from Various Sources. *Energy Fuels* **2000**, *14*, 677-684.

25. Mullins, O. C. The modified yen model. *Energy Fuels* **2010**, *24*, 2179-2207.

26. Qian, K.; Edwards, K. E.; Mennito, A. S.; Freund, H.; Saeger, R. B.; Hickey, K. J.; Francisco, M. A.; Yung, C.; Chawla, B.; Wu, C.; Kushnerick, J. D.; Olmstead, W. N. Determination of structural building blocks in heavy petroleum systems by collision-induced dissociation fourier transform ion cyclotron resonance mass spectrometry. *Anal. Chem.* **2012**, *84*, 4544-4551.

27. Karimi, A.; Qian, K.; Olmstead, W. N.; Freund, H.; Yung, C.; Gray, M. R. Quantitative evidence for bridged structures in asphaltenes by thin film pyrolysis. *Energy Fuels* **2011**, *25*, 3581-3589.

28. Gray, M. R. Consistency of asphaltene chemical structures with pyrolysis and coking behavior. *Energy Fuels* **2003**, *17*, 1566-1569.

29. Siskin, M.; Kelemen, S. R.; Eppig, C. P.; Brown, L. D.; Afeworki, M. Asphaltene molecular structure and chemical influences on the morphology of coke produced in delayed coking. *Energy Fuels* **2006**, *20*, 1227-1234.

30. Ancheyta, J.; Betancourt-Rivera, G.; Marroquin-Sanchez, G.; Perez-Arellano, A. M.; Maity, S. K.; Cortez, M. T.; del Rio-Soto, R. An exploratory study for obtaining synthetic crudes from heavy crude oils via hydrotreating. *Energy Fuels* **2001**, *15*, 120-127.

31. Ancheyta, J.; Betancourt, G.; Centeno, G.; Marroquin, G.; Alonso, F.; Garciafigueroa, E. Catalyst deactivation during hydroprocessing of Maya heavy crude oil. 1. Evaluation at constant operating conditions. *Energy Fuels* **2002**, *16*, 1438-1443.

32. Ancheyta, J.; Betancourt, G.; Marroquín, G.; Centeno, G.; Castañeda, L. C.; Alonso, F.; Muñoz, J. A.; Gómez, M. T.; Rayo, P. Hydroprocessing of Maya heavy crude oil in two reaction stages. *Applied Catalysis A: General* **2002**, *233*, 159-170.

33. Sorokina, T. P.; Buluchevskaya, L. A.; Potapenko, O. V.; Doronin, V. P. Conversion of nickel and vanadium porphyrins under catalytic cracking conditions. *Petroleum Chemistry* **2010**, *50*, 51-55.

34. Yen, T. F. In *Chemical aspects of metals in native petroleum;* Yen, T. F., Ed.; The Role of Trace Metals in Petroleum; Ann Arbor Science: Ann Arbor, MI, 1975; pp 1-30.

35. Filby, R. H. In *The nature of metals in petroleum;* Yen, T. F., Ed.; The Role of Trace Metals in Petroleum; Ann Arbor Science: Ann Arbor, MI, 1975; pp 31-58.

36. Ali, M. F.; Perzanowski, H.; Bukhari, A.; Al-Haji, A. Nickel and vanadyl porphyrins in Saudi Arabian crude oils. *Energy Fuels* **1993**, *7*, 179-184.

37. Miller, J. T.; Fisher, R. B.; van, d. E.; Koningsberger, D. C. Structural determination by xafs spectroscopy of non-porphyrin nickel and vanadium in maya residuum, hydrocracked residuum, and toluene-insoluble solid. *Energy Fuels* **1999**, *13*, 719-727.

38. Strausz, O. P.; Lown, E. M. *The Chemistry of Alberta Oil Sands, Bitumens and Heavy Oils;* Alberta Energy Research Institute: Calgary, AB, 2003.

39. Yin, C.; Stryker, J. M.; Gray, M. R. Separation of petroporphyrins from asphaltenes by chemical modification and selective affinity chromatography. *Energy Fuels* **2009**, *23*, 2600-2605.

40. Zhao, X.; Liu, Y.; Xu, C.; Yan, Y.; Zhang, Y.; Zhang, Q.; Zhao, S.; Chung, K.; Gray, M. R.; Shi, Q. Separation and characterization of vanadyl porphyrins in Venezuela Orinoco heavy crude oil. *Energy Fuels* **2013**, *27*, 2874-2882.

41. Hodgson, G. W.; Hitchon, B.; Elofson, R. M.; Baker, B. L.; Peake, E. Petroleum pigments from Recent fresh-water sediments. *Geochim. Cosmochim. Acta* **1960**, *19*, 272-288.

42. Hodgson, G. W.; Hitchon, B.; Taguchi, K.; Baker, B. L.; Peake, E. Geochemistry of porphyrins, chlorins and polycyclic aromatics in soils, sediments and sedimentary rocks. *Geochim. Cosmochim. Acta* **1968**, *32*, 737-772.

43. Blumer, M.; Omenn, G. S. Fossil porphyrins: uncomplexed chlorins in a triassic sediment. *Geochim. Cosmochim. Acta* **1961**, *25*, 81-90.

44. Dunning, H. N.; Moore, J. W.; Myers, A. T. Properties of porphyrins in petroleum. *Ind. Eng. Chem.* **1954**, *46 (9)*, 2000-2007.

45. Horeczy, J. T.; Hill, B. N.; Walters, A. E.; Schutze, H. G.; Bonner, W. H. Determination of trace metals in oils. *Anal. Chem.* **1955**, *27*, 1899-1903.

46. Premović, P. I.; Nikolić, N. D.; Tonsa, I. R.; Pavlović, M. S.; Premović, M. P.; Dulanović, D. T. Copper and copper(II) porphyrins of the Cretaceous–Tertiary boundary at Stevns Klint (Denmark). *Earth Planet. Sci. Lett.* **2000**, *177*, 105-118.

47. Cordeiro, M. R.; Moreira, W. C. Thermal behavior of tetrapyrrole derivatives and their mixed complexes. *Thermochim. Acta* **2009**, *486*, 52-56.

48. Gamboa, M.; Campos, M.; Torres, L. A. Study of the stability of 5,10,15,20-tetraphenylporphine (TPP) and metalloporphyrins NiTPP, CoTPP, CuTPP, and ZnTPP by differential scanning calorimetry and thermogravimetry. *Journal of Chemical Thermodynamics* **2010**, *42*, 666-674.

49. Hughey, C. A.; Rodgers, R. P.; Marshall, A. G. Resolution of 11 000 compositionally distinct components in a single electrospray ionization fourier transform ion cyclotron resonance mass spectrum of crude oil. *Anal. Chem.* **2002**, *74*, 4145-4149.

50. Speight, J. G. Visbreaking: A technology of the past and the future. *Sci. Iranica* **2012**, *19*, 569-573.

51. Fairburn, J. A.; Behie, L. A.; Svrcek, W. Y. Ultrapyrolysis of n-hexadecane in a novel micro-reactor. *Fuel* **1990**, *69*, 1537-1545.

52. Cartlidge, C. R.; Dukhedin-Lalla, L.; Rahimi, P.; Shaw, J. M. Preliminary phase diagrams for ABVB + n-dodecane + hydrogen. *Fluid Phase Equilib.* **1996**, *117*, 257-264.

53. Olmstead, W. N.; Freund, H. Thermal Conversion Kinetics of Petroleum Residua. *AIChE Spring National Meeting*, New Orleans, LA. **1998**.

54. McMillen, D. F.; Golden, D. M. Hydrocarbon bond dissociation energies. *Annu. Rev. Phys. Chem.* **1982**, *33*, 493-532.

55. Campbell, J. D.; Teymour, F.; Morbidelli, M. High temperature free radical polymerization. 1. Investigation of continuous styrene polymerization. *Macromolecules* **2003**, *36*, 5491-5501.

56. Poutsma, M. L. Fundamental reactions of free radicals relevant to pyrolysis reactions. *J. Anal. Appl. Pyrolysis* **2000**, *54*, 5-35.

57. Khorasheh, F.; Gray, M. R. High-pressure thermal cracking of n-hexadecane. *Industrial and Engineering Chemistry Research* **1993**, *32*, 1853-1863.

58. Khorasheh, F.; Gray, M. R. High-pressure thermal cracking of n-hexadecane in aromatic solvents. *Industrial and Engineering Chemistry Research* **1993**, *32*, 1864-1876.

59. Khorasheh, F.; Gray, M. R. High-pressure thermal cracking of n-hexadecane in tetralin. *Energy Fuels* **1993**, *7*, 960-967.

60. Wu, G.; Katsumura, Y.; Matsuura, C.; Ishigure, K.; Kubo, J. Comparison of liquid-phase and gas-phase pure thermal cracking of n-hexadecane. *Industrial and Engineering Chemistry Research* **1996**, *35*, 4747-4754.

61. Gray, M. R.; Assenheimer, G.; Boddez, L.; McCaffrey, W. C. Melting and fluid behavior of asphaltene films at 200-500 C. *Energy Fuels* **2004**, *18*, 1419-1423.

62. Moschopedis, S. E.; Parkash, S.; Speight, J. G. Thermal decomposition of asphaltenes. *Fuel* **1978**, *57*, 431-434.

63. Wu, G.; Katsumura, Y.; Matsuura, C.; Ishigure, K.; Kubo, J. Radiation effect on the thermal cracking of n-hexadecane. 2. A kinetic approach to chain reaction. *Industrial and Engineering Chemistry Research* **1997**, *36*, 3498-3504.

64. Domine, F. Kinetics of hexane pyrolysis at very high pressures. 1. Experimental study. *Energy Fuels* **1989**, *3*, 89-96.

65. Domine, F.; Marquaire, P.; Muller, C.; Come, G. Kinetics of hexane pyrolysis at very high pressures. 2. Computer modeling. *Energy Fuels* **1990**, *4*, 2-10.

66. Freund, H.; Olmstead, W. N. Detailed chemical kinetic modeling of butylbenzene pyrolysis. *Int. J. Chem. Kinet.* **1989**, *21*, 561-574.

67. Viskolcz, B.; Seres, L. Ab initio study on alkyl radical decomposition and alkyl radical addition to olefins. *Reaction Kinetics and Catalysis Letters* **2009**, *96*, 245-262.

68. Poutsma, M. L. Comparison of mechanistic models for correlation of activation energies of liquid-phase addition of carbon-centered radicals to terminal olefins. *Journal of Physical Organic Chemistry* **2008**, *21*, 758-782.

69. Fischer, H.; Radom, L. Factors controlling the addition of carbon-centered radicals to alkenes - An experimental and theoretical perspective. *Angewandte Chemie - International Edition* **2001**, *40*, 1340-1371.

70. Smith, C. M.; Savage, P. E. Reactions of polycyclic alkylaromatics. 2. Pyrolysis of 1,3-diarylpropanes. *Energy Fuels* **1991**, *5*, 146-155.

71. Smith, C. M.; Savage, P. E. Reactions of polycyclic alkylaromatics. 4. Hydrogenolysis mechanisms in 1-alkylpyrene pyrolysis. *Energy Fuels* **1992**, *6*, 195-202.

72. Smith, C. M.; Savage, P. E. Reactions of polycyclic alkylaromatics—VI. Detailed chemical kinetic modeling. *Chemical Engineering Science* **1994**, *49*, 259-270.

73. Freund, H.; Matturro, M. G.; Olmstead, W. N.; Reynolds, R. P.; Upton, T. H. Anomalous side-chain cleavage in alkylaromatic thermolysis. *Energy Fuels* **1991**, *5*, 840-846.

74. Dente, M.; Ranzi, E. M. In *Mathematical Modeling of Hydrocarbon Pyrolysis Reactions*; Albright, L. F., Crynes, B. L. and Corcoran, W. H., Eds.; **Pyrolysis: Theory and Industrial Practice**; Academic Press: New York, 1983; pp 133-175.

75. Gray, M. R. *Upgrading Petroleum Residues and Heavy Oils*; Marcel Dekker: New York, NY, 1994.

76. Whitson, C. H.; Brule, M. R. *Phase behavior*; SPE Monograph Series; Society of Petroleum Engineers: Richardson, TX, 2000; Vol. 20, pp 47-67.

77. Firoozabadi, A. *Thermodynamics of Hydrocarbon Reservoirs*; McGraw-Hill: New York, NY, 1999.

78. Peng, D.; Robinson, D. B. A New Two-Constant Equation of State. *Ind. Eng. Chem. Fund.* **1976**, *15*, 59-64.

79. Prausnitz, J. M.; Lichtenthaler, R. N.; Gomes de Azevedo, E. *Molecular Thermodynamics of Fluid-Phase Equilibria;* Prentice Hall: Upper Saddle River, NJ, 1999.

80. Oldenburg, T. B. P.; Huang, H.; Donohoe, P.; Willsch, H.; Larter, S. R. High molecular weight aromatic nitrogen and other novel hopanoid-related compounds in crude oils. *Org. Geochem.* **2004**, *35*, 665-678.

81. Mierau, J. Patterns and pathways of hydrogenation of asphaltene model compounds, University of Alberta, Edmonton, 2011.

82. MestReNova 6.0, Mestrelab Research, Santiago de Compostela, Spain.

83. Duncan, M. W.; Roder, H.; Hunsucker, S. W. Quantitative matrix-assisted laser desorption/ionization mass spectrometry. *Brief Funct Genomic Proteomic* **2008**, *7(5)*, 355-370.

84. Dunn, J. G.; Sharp, J. H. In *Thermogravimetry;* Kolthoff, I. M., Elving, P. J., Eds.; Treatise on Analytical Chemistry; John Wiley & Sons: New York, NY, 1993; Vol. 13, pp 127-266.

85. Alshareef, A. H.; Azyat, K.; Tykwinski, R. R.; Gray, M. R. Measurement of cracking kinetics of pure model compounds by thermogravimetric analysis. *Energy Fuels* **2010**, *24*, 3998-4004.

86. Wei, X.; Du, X.; Chen, D.; Chen, Z. Thermal analysis study of 5,10,15,20-tetrakis (methoxyphenyl) porphyrins and their nickel complexes. *Thermochim. Acta* **2006**, *440*, 181-187.

87. Lebedeva, N. S.; Pavlycheva, N. A.; V'yugin, A. I. Kinetics of thermal oxidative decomposition of zinc porphyrin and phthalocyanine complexes. *Russ. J. Gen. Chem.* **2007**, *77*, 629-640.

88. Poutsma, M. L. Free-radical thermolysis and hydrogenolysis of model hydrocarbons relevant to processing of coal. *Energy Fuels* **1990**, *4*, 113-131.

89. VMGSim 7.0, Virtual Materials Group Inc., Calgary, AB.

90. Lecat, M. Azeotropes of Ethyl Urethane and other Azeotropes. *C. R. Hebd. Seances Acad. Sci.* **1943**, *217*, 273.

91. Sax, N. I. *Dangerous Properties of Industrial Materials;* VanNostrand Reinhold Company: New York, 1979; pp 1118.

92. Laane, J.; Haller, K.; Sakurai, S.; Morris, K.; Autrey, D.; Arp, Z.; Chiang, W.; Combs, A. Raman spectroscopy of vapors at elevated temperatures. *J. Mol. Struct.* **2003**, *650*, 57-68.

93. Lide, D. R., Ed.; In *CRC Handbook of Chemistry and Physics;* CRC Press: Boca Raton, FL, 2003; pp 2616.

94. Stewart, A. W.; McVicker, W. H.; Marsh, J. K. CXXXVII. Tesla-luminescence spectra. Part V. Some polynuclear hydrocarbons. *J. Chem. Soc.* **1925**, *127*, 999.

95. Stull, D. R. Vapor Pressure of pure substances, organic and inorganic compounds. *Ind. Eng. Chem.* **1947**, *39*, 517-540.

96. Riedel, L. Eine neue universelle damfdruck-formal (A new universal vapor pressure equation). *Chem. Ing. Tech.* **1954**, *26*, 83.

97. Weast, R. C.; Astle, M. J. *Handbook of Data on Organic Compounds;* CRC Press: Boca Raton, FL, 1985.

98. Yaws, C. L. *Handbook of Vapor Pressure;* Gulf Publishing Co.: Houston, TX, 1994; Vol. 1-3.

99. Design Institute for Physical Properties, Sponsored,by AIChE DIPPR Project 801 - Full Version.

100. Savage, P. E.; Jacobs, G. E.; Javanmardian, M. Autocatalysis and aryl-alkyl bond cleavage in 1-dodecylpyrene pyrolysis. *Ind. Eng. Chem. Res.* **1989**, *28*, 645-654.

101. Freund, H.; Olmstead, W. N. Detailed chemical kinetic modeling of butylbenzene pyrolysis. *Int. J. Chem. Kinet.* **1989**, *21*, 561-574.

102. Ahluwalia, V. K.; Parashar, R. K. *Organic Reaction Mechanisms;* Alpha Science International: Harrow, Middlesex, 2005; pp 78-136.

103. De Vleeschouwer, F.; Jaque, P.; Geerlings, P.; Toro-Labbe, A.; De Proft, F. Regioselectivity of radical additions to substituted alkenes: Insight from conceptual density functional theory. *J. Org. Chem.* **2010**, *75*, 4964-4974.

104. De, M., A.; Margarita, R.; Mariani, A.; Piancatelli, G. Radical additions to olefins in the presence of iodobenzenediacetate: an easy route to alkyl dithiocyanates. *Tetrahedron Lett.* **1996**, *37*, 1889-1889.

105. Moore, L. O. Radical reactions of highly polar molecules. Relative reactivity of halogenated olefins in haloalkyl radical additions. *J. Phys. Chem.* **1970**, *74*, 3603-3607.

106. Giese, B. *Radicals in Organic Synthesis: Formation of Carbon-Carbon Bonds;* Pergamon Press: Oxford, 1986; pp 14-17.

107. Fleming, I. *Frontier Orbitals and Organic Chemical Reactions;* Wiley: New York, 1976; pp 182-207.

108. Evans, A. G.; George, D. B. 910. The catalytic action of anionic catalysts. Part I. The interaction of butyl-lithium with 1,1-diphenylethylene. *J. Chem. Soc.* **1961**, *0*, 4653-4659.

109. Yuki, H.; Kato, M.; Okamoto, Y. Anionic copolymerization of styrene and trans-stilbene with n- butyllithium. *Bull. Chem. Soc. Jpn.* **1968**, *41*, 1940-1944.

110. Cameron, G. G.; Grassie, N. The thermal depolymerization of polystyrene. V. Styrene - stilbene copolymers. *Makromol. Chem.* **1962**, *51*, 130-136.

111. Ruchardt, C.; Gerst, M.; Nolke, M. The uncatalyzed transfer hydrogenation of alpha-methylstyrene by dihydroanthracene or xanthene - a radical reaction. *Angew. Chem. Int. Ed Engl.* **1992**, *31*, 1523-1525.

112. Morgenthaler, J.; Ruchardt, C. New Hydrogen Transfer Catalysts. *Eur. J. Org. Chem.* **1999**, 9, 2219-2230.

113. Peng, M. Thermal cracking of asphaltene by addition of hydrogen donor solvent, University of Alberta, Edmonton, 2012.

114. Habib, F.; Diner, C.; Stryker, J.; Semagina, N.; Gray, M. *Suppression of addition reactions of asphaltene model compounds during hydrogenation reaction by using iron sulfide catalyst.* Poster session presented at the 14th International Conference on Petroleum Phase Behavior and Fouling, Rueil-Malmaison, France. **2013, June**.
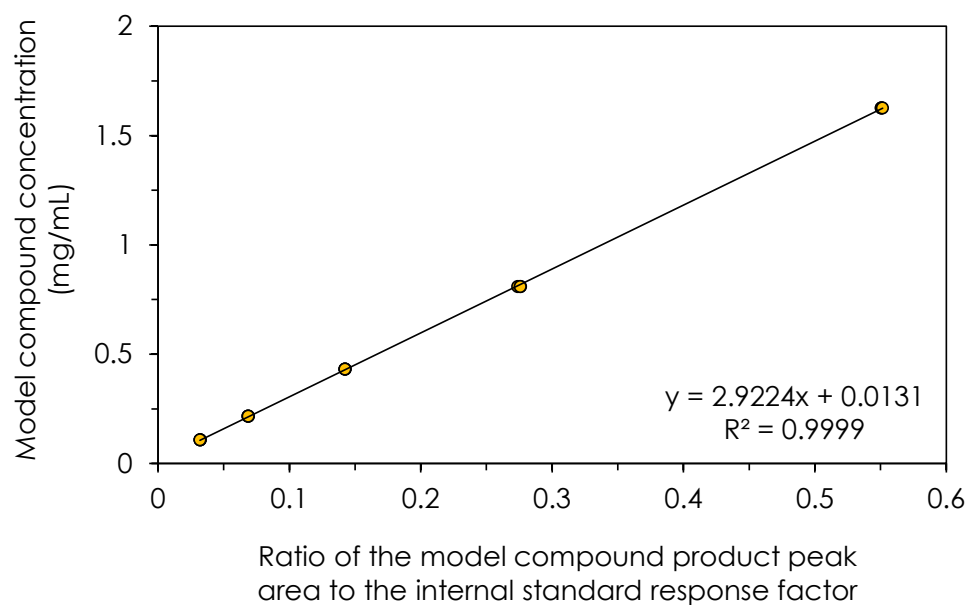
APPENDIX A:

HPLC Calibration Curves

HPLC calibration curves were constructed for both model compounds, [Et-Py]NiTPP and 2[Et-Py]NiTPP, using NiTPP as the internal standard and measured peak areas at a wavelength of 414 nm. Calibration curves were made by tabulating the peak areas of the model compound and internal standard in samples with a known quantity of analyte at 4 to 5 different concentrations. HPLC chromatograms were collected 3 times for each calibration sample. Once the data was collected, the calibration curves were built by plotting the model compound concentration vs. the ratio of the model compound peak area to the internal standard response factor. The internal standard response factor is defined as the ratio between the internal standard peak area and the internal standard concentration. Figure A-1 and Figure A-2 show the HPLC calibration curve of [Et-Py]NiTPP and 2[Et-Py]NiTPP, respectively, along with the resulting linear regression equations which were used to calculate model compound concentrations after reaction.

$y = 2.1498x + 0.0099$
$R^2 = 0.9999$
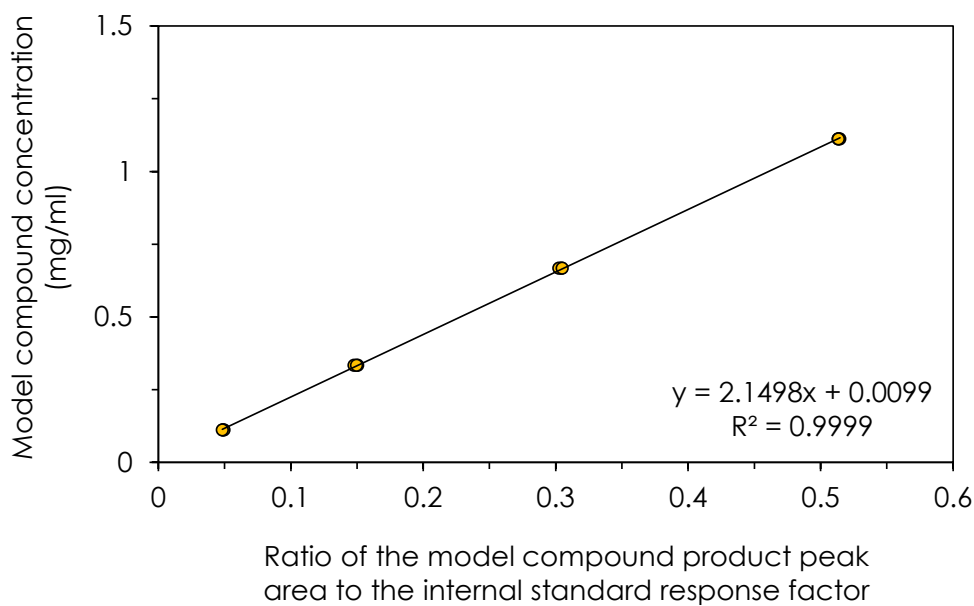
Figure A-1. HPLC calibration curve of [Et-Py]NiTPP

$y = 2.9224x + 0.0131$
$R^2 = 0.9999$

Figure A-2. HPLC calibration curve of 2[Et-Py]NiTPP

APPENDIX B:

Yield of Coupling Product

A combination of the data from HPLC and MALDI-MS were used to determine the yield of the olefin-model compound coupling product. For example, for reaction of [Et-Py]NiTPP with 1-C_{16} at 375 °C for 20 min, Figure B-1 shows a representative MALDI mass spectrum of the reaction products; a minimum of 9 spectrums were collected for each sample to minimize variability in the data collected. Then, for each spectrum, the sum of the corresponding peak heights for both model compound and coupling product were tabulated, including those of their corresponding isotopes. Table B-1 shows the data for this particular reaction sample. Finally, using the average value of the ratio of peak intensities, 0.109±0.006, the model compound conversion determined by HPLC, 24.9%, and assuming the same ionization efficiency for both compounds on a molar basis, the yield of the coupling product can be calculated, giving a value of 28.2 mol/100 mol of converted model compound.
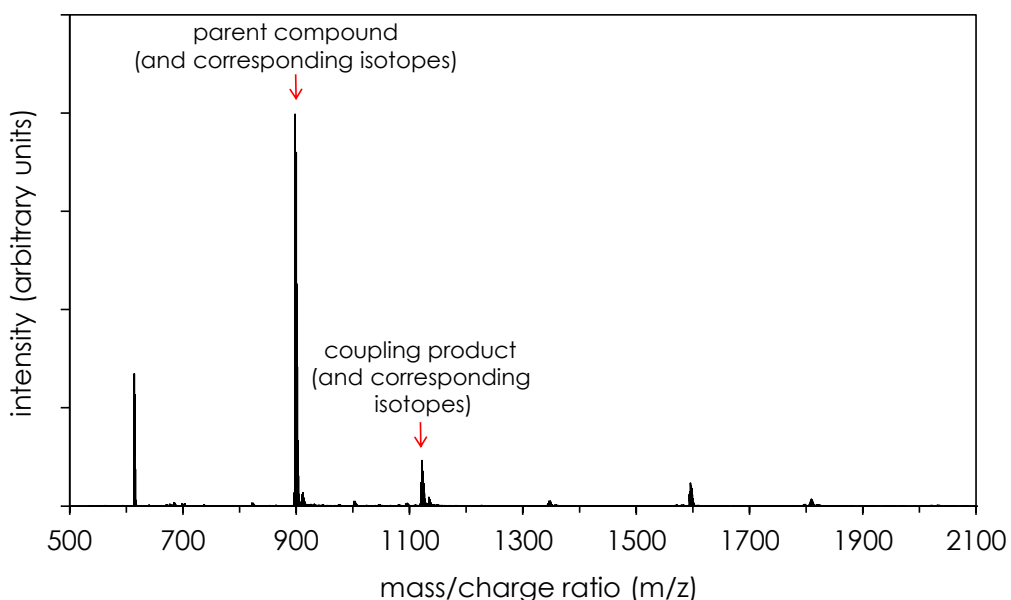
Figure B-1. MALDI mass spectrum of products from thermal cracking of [Et-Py]NiTPP with 1-C_{16} at 375 °C for 20 min. Spectrum shows the parent compound at m/z 898.0 and the formation of the coupling product at m/z 1122.2 (and their corresponding isotope peaks).

Table B-1. Intensity of the model compound and coupling product peaks, including isotopes, from the MALDI mass spectrum shown in Figure B-1

Spectrum	Sum of intensities (arbitrary units)		Ratio of intensities
	[Et-Py]NiTPP	Coupling product	
1	183417	19529	0.11
2	59351	6552	0.11
3	133770	14779	0.11
4	105883	10593	0.10
5	75128	7881	0.10
6	67867	8124	0.12
7	48433	5550	0.11
8	74631	7872	0.11
9	50937	5601	0.11
		Average	0.109±0.006